Journal : SmallExtended 10651	Article No : 632	Pages : 36	MS Code : 632	Dispatch : 13-11-2024

Environmental and Ecological Statistics
https://doi.org/10.1007/s10651-024-00632-8

A hierarchical model for eDNA fate and transport dynamics accommodating low concentration samples

Ben C. Augustine[1] · Patrick R. Hutchins[1] · Devin N. Jones[1] · Jacob R. Williams[2] · Eric Leinonen[2] · Adam J. Sepulveda[1]

Received: 4 April 2024 / Revised: 12 September 2024 / Accepted: 5 October 2024

Abstract

Environmental DNA (eDNA) sampling is an increasingly important tool for answering ecological questions and informing aquatic species management; however, several factors currently limit the reliability of ecological inference from eDNA sampling. Two particular challenges are (1) determining species source location(s) and (2) accurately and precisely measuring low concentration eDNA samples in the presence of multiple sources of ecological and measurement variability. The recently introduced eDNA Integrating Transport and Hydrology (eDITH) model provides a framework for relating eDNA measurements to source locations in riverine networks, but little empirical work has been done to test and refine model assumptions or accommodate low concentration samples, that can be systematically undermeasured. To better understand eDNA fate and transport dynamics and our ability to reliably quantify low concentration samples, we developed a hierarchical model and used it to evaluate a fate and transport experiment. Our model addresses several low concentration challenges by modeling the number of copies in each PCR replicate as a latent variable with a count distribution and conditioning detection and quantification on replicate copy number. We provide evidence that the eDNA removal rate declined through time, estimating that over 80% of eDNA was removed over the first 10 m, traversed in 41 s. After this initial period of rapid decay, eDNA decayed slowly with consistent detection through our farthest site 1 km from the release location, traversed in 67.8 min. Our model further allowed us to detect extra-Poisson variation in the allocation of copies to replicates. We extended our hierarchical model to accommodate a continuous effect of inhibitors and used our model to provide evidence for the inhibitor hypothesis and explore the potential implications. While our model is not a panacea for all challenges faced when quantifying low-concentration eDNA samples, it provides a framework for a more complete accounting of uncertainty.

A1 Handling Editor: Luiz Duczmal.

A2 Extended author information available on the last page of the article

Journal : SmallExtended 10651	Article No : 632	Pages : 36	MS Code : 632	Dispatch : 13-11-2024

Keywords eDNA inhibitors · eDNA survival · eDNA transport · Environmental DNA · Hierarchical modeling

1 Introduction

Environmental DNA (eDNA) approaches are increasingly being used to estimate ecological parameters like species distributions (Carraro et al. 2018), abundance (Rourke et al. 2022), and phenology (Searcy et al. 2022) due to their detection sensitivity, wide applicability across species, and cost efficiency, among other reasons (Jo and Yamanaka 2022). Further, eDNA sampling can be a particularly useful tool for aquatic invasive species monitoring, potentially allowing for early detection and eradication (Larson et al. 2020; Morisette et al. 2021; Sepulveda et al. 2020). However, across many applications of eDNA monitoring in aquatic environments, the reliability of ecological inference can be reduced by (1) uncertainty in the source location of detected eDNA (Carraro et al. 2018; Jo and Yamanaka 2022) and (2) difficulties measuring site and sample eDNA concentrations with minimal bias while accounting for all relevant sources of uncertainty (Ellison et al. 2006; Shelton et al. 2019; Espe et al. 2022). Both of these factors have the potential to reduce the effectiveness of eDNA sampling for management action, depending on their magnitude and how well they are addressed in experimental/monitoring design and statistical analysis.

A key requirement for many aquatic applications of eDNA sampling, particularly for invasive species monitoring, is to estimate source population locations because the location where eDNA is detected is not necessarily where it was produced due to hydrological transport (Carraro et al. 2018; Burian et al. 2021; Jo and Yamanaka 2022). In stream or river networks, eDNA flows downstream from the source(s) and is detectable until the eDNA concentration attenuates below a detectable level due to physical degradation (Lance et al. 2017) and/or removal from the water column (Shogren et al. 2017). Therefore, an understanding of eDNA transport dynamics is required to either localize source populations (e.g., Carraro et al. 2018) or more broadly, estimate the plausible range of upstream distances a source population can be located from a detection to direct next steps, like more intensive sampling for confirmation (Sepulveda et al. 2023).

Environmental DNA fate and transport dynamics are the product of (1) ecological and biological factors determining how much eDNA is produced across source populations (e.g., abundance, biomass, eDNA production rate), (2) hydrological factors (e.g., discharge, particle settling and resuspension, river network connectivity), and (3) their interaction (e.g., eDNA degradation, removal from water column to substrate) (Carraro et al. 2018; Curtis et al. 2021; Troth et al. 2021; Shogren et al. 2017). A recent modeling framework that includes these general features is the eDNA Integrating Transport and Hydrology (eDITH) model (Carraro et al. 2018, 2021), which has been used to predict the locations of source populations and their eDNA production rates (Carraro et al. 2021) that can correlate with abundance (Jo and Yamanaka 2022). The eDITH model is necessarily simplistic, given the number of factors that need to be accounted for with

the typical level of eDNA sampling and the need to apply the model to large river networks which can be computationally intensive. Further, the eDITH model likelihood can be multimodal (described as "equifinality" by Carraro et al. 2021), with the eDNA removal rate parameter(s), the product of both physical decay and removal, being poorly estimated (Carraro et al. 2021). Therefore, prior information, particularly about the eDNA removal rate parameter(s), can improve parameter estimation and thus ecological inference (Carraro et al. 2021, 2023).

Release experiments (e.g., Jane et al. 2015; Laporte et al. 2020,) have been important for improving understanding of eDNA transport and removal dynamics, and they offer a means of providing parameter estimates that can be used as prior information in future modeling when the source locations are not known in advance (e.g., Carraro et al. 2018). Further, release experiments allow us to test model assumptions (Bylemans et al. 2018; Yates et al. 2021), better evaluate the level of realism necessary for reliable inference, and assess the data demands for a given level of realism. For example, eDITH model applications to date have assumed that the eDNA removal rate is constant with respect to time, which could lead to biased estimates of source locations or detection distance from a source if violated. In fact, the eDNA removal rate has been shown to decline with time in some experiments (Bylemans et al. 2018; Yao et al. 2022; Snyder et al. 2023). Bylemans et al. (2018) hypothesized this decline may be due to variable removal rates across eDNA fragments, such as between fragments in cells and free-floating DNA, and Snyder et al. (2023) provided experimental evidence that removal rate varies by particle size. To our knowledge, these hypotheses have not been compared to empirical data within the eDITH framework, which is possible in release experiments if the relevant hydrological variables are measured accurately.

Another key requirement of many aquatic applications of eDNA sampling is the accurate and precise quantification of eDNA concentration. While many ecological questions can be addressed with eDNA detection data alone (e.g., Hunter et al. 2015), relating eDNA measurements to abundance or modeling eDNA production, transport, and removal as a function of hydrology require quantitative eDNA measurements. These measurements can be obtained by quantitative or digital PCR (Yates et al. 2019), where measurements are made across multiple PCR technical replicates (hereafter 'replicates') of the same sample. These replicate-level measurements are typically then summarized and treated as data, usually using the mean concentration across replicates as the sample concentration or averaging replicates across samples to produce site concentrations (e.g., Yates et al. 2021). However, replicate measurements vary due to multiple factors including variable concentrations across samples (Chambert et al. 2018; Shelton et al. 2019), variability in the allocation of eDNA copies to replicates (Rossmanith and Wagner 2011; Dorazio and Hunter 2015; Tellinghuisen 2020), and measurement error in replicate copy number/concentration (Shelton et al. 2019; Espe et al. 2022). The common approach of averaging replicate concentrations does not partition multiple sources of variance and pools the measurement error with the ecological variance, potentially eroding ecological inference if the measurement error is non-negligible in magnitude relative to ecological variation.

Journal : SmallExtended 10651 | Article No : 632 | Pages : 36 | MS Code : 632 | Dispatch : 13-11-2024

Low concentration samples present several unique challenges for accurate eDNA quantification. First, eDNA copy number or concentration estimates are typically modeled assuming approximate normality (usually on the log scale, see Carraro et al. 2018; Espe et al. 2022), which is an accurate approximation at high concentrations where copy numbers in replicates are large, but less so as concentrations decline and there are few copies per replicate (Ellison et al. 2006; Dorazio and Hunter 2015). Further, copy number measurements are often censored from below by a fixed number of quantitative (q)PCR cycles or a limit of quantification or limit of blank, which requires lower truncation of the observation model distribution (Espe et al. 2022). Low concentration samples also present challenges for interpreting nondetections—as sample concentrations decline, both true negative (Poisson sampling zeros) and false negative (failed detections) replicates become more likely, which cannot be deterministically separated given the observed data (Ellison et al. 2006). In this situation, excluding zeros from sample means will introduce positive bias, while including them may also introduce bias, with the direction depending on the relative proportion of true and false negatives. Finally, sample concentration can be underestimated due to interference by eDNA inhibitory compounds in water samples (i.e., inhibition), which can be difficult to reliably detect (Kontanis and Reed 2006; Lance and Guan 2020), and these inhibitors are more likely to affect lower concentration samples (McKee et al. 2015; Hunter et al. 2019). Such underestimation can bias ecological inference–for example, the eDNA removal rate in a release experiment would be overestimated or the source location prediction from an eDITH model would be too far away. These challenges for quantifying low concentration samples are of particular concern when the goal is the early detection of invasive species, which are easiest to eradicate when population sizes are small, yet those populations produce less eDNA, yielding more samples where quantitative measurements are unreliable.

Hierarchical models are useful for partitioning multiple sources of variation and reducing bias by allowing the source(s) of bias to be modeled more mechanistically (Royle and Dorazio 2008). These models are increasingly being used in eDNA analyses—for example, multiscale occupancy models (Nichols et al. 2008; Dorazio and Erickson 2018; Stratton et al. 2020) have been used to propagate uncertainty in replicate-level occupancy states to site occupancy estimates and covariate relationships, and occupancy models have been extended to account for false positives (e.g., Smith and Goldberg 2020; Guillera-Arroita et al. 2017). Hierarchical models have been used for quantitative eDNA data to partition measurement and multiple levels of environmental variation and relate both detection and quantitative measurements to site concentration (Shelton et al. 2019; Espe et al. 2022). However, to deal with the challenges of low concentration eDNA measurement, a hierarchical model representing the replicate copy numbers as latent discrete random variables may provide improved inference. In such a model, the copy numbers can be assigned a more appropriate count distribution, and the uncertainty in whether observed zeros are true or false negatives can be propagated to the ecological parameters of interest. Further, representing the copy numbers directly in the model may improve our ability to assess lack of fit at the replicate level and investigate hypotheses about inhibitors affecting the replicate-level measurements.

Journal : SmallExtended 10651	Article No : 632	Pages : 36	MS Code : 632	Dispatch : 13-11-2024

To better understand eDNA transport/removal, environmental variation, measurement error, and our ability to jointly estimate the parameters of these processes, we conducted an eDNA release experiment and developed a hierarchical model to apply to our experimental data that accommodates all three sources of nondetections described above (no copies allocated to a replicate, copies allocated but not detected, and copies allocated and detected, but measurement censored and treated as a nondetection). Of particular concern was how well the eDITH model parameters are estimated and whether the eDNA removal rate is constant or declining through time. Because we observed that our original model did not adequately fit our experimental data, particularly for lower concentration samples, we hypothesized that the source of poor fit could be eDNA inhibitory compounds and expanded the model to accommodate the impact of eDNA inhibitors on detection and copy number quantification. We used this model to illustrate how inhibitors can bias inference of multiple parameters and demonstrate how they can, in principle, be accommodated through hierarchical modeling for more reliable ecological inference.

2 Field methods

2.1 DNA release

We conducted this experiment in the upper section of a 1st-order tributary of the Gallatin River located on the Flying D Ranch in southwest Montana (USA), 2023 August 21–24. The upper section of this stream is approximately 1 m wide, 3–12 cm deep, a gradient of 50 m/km, had a mean discharge 0.02 (m^3/s) during our study and flows into a small reservoir containing a conservation brood stock of Arctic grayling (*Thymallus arcticus*), the target species for this study. An artificial barrier restricts upstream movement of Arctic grayling from the reservoir into the study reach—this species is absent in the watershed upstream of the barrier. We introduced water collected from the reservoir's offshore zone to the injection point (0 m) at the top of the 1000 m study reach; a plunge pool occurred immediately downstream of the injection point and putatively helped to mix introduced DNA. This experimental water was transported from the reservoir in ~ 200 L carboys and then transferred into bleached and rinsed coolers connected in series and placed in a shaded area adjacent to the injection point. The water was refreshed every 12 h. Beginning at time 0 h, water was dripped into the stream at a rate of 220 mL/min for 49 h using an electric-operated pump connected to the cooler series and 2.5-cm PVC that spanned the width of the stream. Eight sprinkler emitters were attached to the PVC at 0.1 m intervals so that experimental water was dripped across the stream's width to facilitate mixing. At time 32 h, eight Arctic grayling that were recreationally-angled and legally harvested were added to the cooler series. Experimental water was dripped into the stream until eDNA sampling concluded.

Journal : SmallExtended 10651	Article No : 632	Pages : 36	MS Code : 632	Dispatch : 13-11-2024

2.2 eDNA sampling

At time 48 h, we used distinct 19-L buckets to collect eDNA samples at −0.5, 0.5, 2.5, 5, 10, 20, 40, 80, 125, 200, 300, 400, 500, 1000 m from the injection point. Sampling was completed at all sites within 5 min. Buckets were bleached (50% commercial bleach, Goldberg et al. 2016), rinsed with stream water upstream of the injection point, and then repeatedly rinsed with stream water at the sampling point prior to collecting a sample. To collect samples, we filled the bucket with stream water from the cross-section midpoint, swirled the bucket, and then poured this water into each of six, 1-L sterile whirlpak bags. Our intention with the buckets was to collect uniform samples at and across sampling points in as short a time-increment as possible to minimize any temporal variability associated with inconsistent eDNA production and removal rates. Bags were stored at ambient temperatures in the shade and filtered on site through 47-mm diameter, 1.2 µm mixed cellulose ester filters (Millipore) within 90 min of collection. Filters were placed immediately into 200 µL lysis buffer, which contained 20 µL of proteinase K and 180 µL of Qiagen Buffer AE, and returned to USGS Northern Rocky Mountain Science Center (NOROCK) for extraction and analysis.

We collected two field negative controls immediately before time 48 h, which consisted of 250-mL of deionized water poured into sterilized whirlpak bags. We collected field positive controls by sampling 1 L of water directly from the reservoir at time −24 and 0 h, and by sampling 1 L of water from the coolers at time 0, 24, and 48 h. Controls were handled similarly to experimental samples. Negative controls were filtered immediately prior to experimental samples, whereas positive controls were filtered at USGS NOROCK.

2.3 Hydrological covariates

Discharge was measured at all eDNA sample collection sites with the following exceptions due to stream habitat complexity (e.g., undercut banks, large wood and cobbles) that prevented accurate measurement: we used discharge measured at 5 m for the first three sites at 0.5, 2.5 and 5 m; we used discharge measured at 15 m for sites at 10 and 20 m; and we used discharge measured at 35 m for the site at 40 m. Discharge measurements were estimated using the velocity–area method (Herschy 1993), which involves dividing each site cross-section into multiple subsections (approximately every 1 cm) and measuring the width, depth, and flow velocity of each subsection with a hand-held current meter. Discharge values for each subsection were summed to arrive at the cross-section discharge. Discharge was sampled at time 24 h and time 49 h. We also deployed barometric pressure transducers (Onset HOBO water level logger) set to 1-h intervals in the air and water at 125 m to evaluate whether the water surface elevation (as a proxy for discharge) was stable throughout our experiment. The transducer in the water also collected water temperature at hourly increments. We deployed additional

water temperature loggers (Onset HOBO pendant) at −0.5 and 1000 m to describe water temperature at hourly increments.

3 Lab methods

3.1 Inhibition assessment

Here, we describe the methods to assess inhibition—all other lab methods are in "Appendix". Inhibition was measured through the use of an exogenous internal positive control (IPC) in every qPCR reaction, including controls (TaqMan^{TM} Exogenous Internal Positive Control Reagents, cat. #4308321). We added 2 µL of VIC-labeled 10x Exo IPC Mix and 0.4 µL 50x Exo IPC DNA per qPCR reaction. Standard dilutions of IPC DNA were not used, so inhibition was assess using quantification cycle (Cq) values determined from the methods described and referenced above. We used ΔCq to describe inhibition of each qPCR reaction on a continuous scale:

$$\Delta Cq_{kp} = Cq_{kp} - \bar{Cq}_{cp}, \tag{1}$$

where ΔCq_{kp} is the difference in IPC Cq_{kp} for qPCR reaction k on plate p and the mean Cq of a set of c uninhibited control samples on plate p ($\bar{Cq}_{cp}$). Said another way, ΔCq_{kp} is the difference between a sample IPC Cq and the mean IPC Cq of a set of uninhibited samples on the same 96-well plate. Uninhibited control samples for each plate included no-template controls (NTCs) and synthetic standards with copy numbers of the target DNA strand < 1000. Positive values of ΔCq_{kp} reflect a delay in Cq, an indication of possible inhibiting effects.

4 Modeling methods

4.1 Data description

Our eDNA detection and quantification data are structured by site, sample, and PCR replicate. Sites are numbered $i = 1, \ldots, I = 13$, each with a distance from the release site, d_i, in sequential order starting at 0.5 m. At each site, samples are numbered $j = 1, \ldots, J = 6$, and for each sample, replicates are numbered $k = 1 \ldots, K = 5$. We define $y^{obs}_{i,j,k}$ to be the measured copy number for site i, sample j, and replicate k, with copy number measurements converted from the observed Cq values. Elements of $\boldsymbol{y}^{obs}$ corresponding to failed detections are set to 0 as are any copy number observations less than a lower bound for quantification, η^q. This quantification lower bound can be set to the copy number corresponding to the maximum number of PCR cycles used to account for data censoring due to a limited cycle number (Espe et al. 2022), or it can be set to exclude the lowest copy number measurements if (1) they do not meet model assumptions (e.g., biased measurement at low concentrations, discussed below), or (2) they are below a limit of blank and may be false positives (Lesperance et al. 2021).

Next, we define $y^{det}_{i,j,k}$ to be the detection data taking value 1 if the copy number measurement is greater than η^d and 0 otherwise, where η^d is a lower bound of detection that is less than or equal to the lower bound of quantification. For our analyses, we set η^q to the copy number corresponding to 50 cycles and we set $\eta^d = 0$ because we expect every sample to contain target eDNA. If false positives are a concern, both η^d and η^q can be set higher, perhaps at the limit of blank (Lesperance et al. 2021). Note, these definitions of detection and quantification lower bounds differ from standard definitions of "limit of detection" and "limit of quantification" (e.g., Klymus et al. 2020). Finally, for the hydrological data, we define Q_i to be the discharge rate at site i and v_i to be the average stream velocity between the release location and site i. Due to concerns about the measurement precision of stream velocity at each site relative to typical variation over a 1 km stream segment, we set the average stream velocity between the release location and each site to the mean of measured velocities across sites: $v_i = \bar{v}$.

4.2 Ecological process model

4.2.1 eDNA production, transport, and removal process

We assume site eDNA concentrations are the product of sub-processes for eDNA production, transport, and removal for which we adapt the eDNA Integrating Transport and Hydrology model (eDITH; Carraro et al. 2018), which is a generalization of mass balance models for single eDNA sources (e.g., Sansom and Sassoubre 2017; Altermatt et al. 2023) to multiple sources that accounts for variable hydrology across sites. The eDITH model is:

$$C_i^{site} = \frac{1}{Q_i} \sum_{j \in \boldsymbol{\gamma}_i} A_j p_{0_j} \exp\left(\frac{-d_{i,j}}{v_{i,j}\tau}\right), \tag{2}$$

where C_i^{site} is the concentration at site i (N/m^3), where N is the number of eDNA copies, Q_i is the water discharge rate at site i (m^3/s), $\boldsymbol{\gamma}_i$ is the set of sites upstream of site i, A_j is the habitat area of site j (m^2), p_{0_j} is the eDNA production rate of site j (N/m^2 s), $d_{i,j}$ is the distance between site i and j (m), $v_{i,j}$ is the mean velocity between site i and j (m/s), and τ is the inverse eDNA removal rate (s). In our experiment, eDNA is added at a point location of zero area, so we remove area and define p_0 to be the eDNA production rate without respect to area with units N/s. Further, eDNA is only "produced" at the release location, removing the need to sum the eDNA contribution of multiple upstream sites. These modifications simplify the eDITH model to:

$$C_i^{site} = \frac{p_0}{Q_i} \exp\left(\frac{-d_i}{v_i \tau}\right), \tag{3}$$

where p_0 is the eDNA production rate at the release location, d_i is the distance between site i and the release location, and v_i is the mean velocity between site i and the release location, which we assume to be constant across sites.

Journal : SmallExtended 10651 | Article No : 632 | Pages : 36 | MS Code : 632 | Dispatch : 13-11-2024

We consider two versions of the eDITH model above with respect to how eDNA is removed from the water column as a function of time. Note that the expected travel time from the release location to site i is $t_i = \frac{d_i}{v_i}$, and the exponential term in the eDITH model is an exponential survival function in continuous time:

$$S(t) = \exp\left(\frac{-t}{\tau}\right). \tag{4}$$

The removal rate is $F(t) = 1 - S(t)$, and we will use this term for better consistency with the eDNA literature. Under an exponential model, DNA is removed at the same rate through time. A Weibull model (David and Mitchel 2012; Bylemans et al. 2018) considers that the eDNA removal rate can increase or decline through time, but includes an extra parameter, which we found led the eDITH model parameters to be too weakly identified for parameter estimation with our data. A power law relationship (Shogren et al. 2017; Levi et al. 2019) allows the eDNA removal rate to decline through time without an extra parameter; however, (1) if we use a power law relationship as a survival function, $S(t) = t^{-\alpha}$, survival goes to infinity when t is less than 1 and (2) without the scale parameter τ, the time units do not cancel. Therefore, we define $T_i = 1 + t_i$, where T is a non-dimensional time factor, and the survival function as a function of T is:

$$S(T) = T^{-\alpha}. \tag{5}$$

This survival function is not derived from a distribution for failure times, such as the exponential or Weibull; however, it may still be empirically adequate to describe faster than exponential decay in our experiment.

The resulting eDITH model with power law eDNA removal in continuous time is then:

$$C_i^{site} = \frac{p_0}{Q_i}\left(1 + \frac{d_i}{v_i}\right)^{-\alpha} \tag{6}$$

for sites 2, … ,13. For both eDITH removal models, we add a thinning parameter at the first site to account for the "plume effect" seen in previous studies (Wood et al. 2020, 2021; Laporte et al. 2020, see Discussion), which describes the phenomenon of delayed mixing with distance from the eDNA source. For example, in the power law version:

$$C_1^{site} = \theta^{site}\frac{p_0}{Q_1}\left(1 + \frac{d_1}{v_1}\right)^{-\alpha}, \tag{7}$$

where $0 < \theta^{site} < 1$. As a consequence, copy number measurements from site 1 do not contribute to the estimation of the eDITH model parameters beyond ensuring that the concentration at site 2 is greater than or equal to that at site 1.

Journal : SmallExtended 10651 | Article No : 632 | Pages : 36 | MS Code : 632 | Dispatch : 13-11-2024

4.2.2 Sampling process

The sampling process describes the variation in sample concentrations collected at a site as a function of the site concentration. This distribution is typically right-skewed due to eDNA clumping in the water column and stochastic collection of more rare, larger "aggregate" particles (Furlan et al. 2016; Yates et al. 2023); therefore, we use a log-normal distribution (Carraro et al. 2018; Espe et al. 2022) to describe this variation. Conditional on the eDNA concentration at site i, we assume that the concentration in each collected sample, $C_{i,j}^{samp}$, varies following:

$$\log\left(C_{i,j}^{samp}\right) \sim \text{Normal}\left(\log\left(C_i^{site}\right), \sigma^{samp}\right), \tag{8}$$

where σ^{samp} is the sampling process standard deviation on the log scale, which could be a function of site covariates such as the distance from the release location.

4.2.3 Replication process

The replication process describes the variability in the number of copies allocated to each replicate given the sample concentration. We model the eDNA copy number in each replicate, $N_{i,j,k}$, as a count random variable with an expected number of copies being a function of the sample concentration (Dorazio and Hunter 2015; Furlan et al. 2016). More specifically,

$$\lambda_{i,j}^{rep} = C_{i,j}^{samp} V_{i,j}^{rep}, \tag{9}$$

where $\lambda_{i,j}^{rep}$ is the expected number of copies in a replicate from site i and sample j and $V_{i,j}^{rep}$ is the sample volume in cubic meters associated with 1 replicate from site i and sample j. If this volume varies across replicates of the same sample, a replicate dimension can be added to $\boldsymbol{\lambda}$ and $\boldsymbol{V}^{rep}$. Next, we assume that the eDNA copies are homogeneously distributed throughout the eDNA extract and deposited into each replicate following a Poisson distribution, which has theoretical support for both digital PCR (dPCR) and qPCR (Dube et al. 2008; Rossmanith and Wagner 2011; Tellinghuisen 2020; Lesperance et al. 2021):

$$N_{i,j,k} \sim \text{Poisson}\left(\lambda_{i,j}^{rep}\right). \tag{10}$$

4.3 Observation model

The observation model describes both the detection and quantification processes. For the detection process, we assume replicate-level detection probability, $p_{i,j,k}^{y}$, is a function of the number of copies in a replicate:

$$\text{logit}\left(p_{i,j,k}^{y}\right) = \gamma_0 + \gamma_1(N_{i,j,k} - 1). \tag{11}$$

Journal : SmallExtended 10651 | Article No : 632 | Pages : 36 | MS Code : 632 | Dispatch : 13-11-2024

By subtracting 1 from the number of copies in each replicate, γ_0 corresponds to the detection probability of 1 copy, and we constrain $\gamma_1 > 0$ with a truncated prior (see Supplementary Materials B). Then, we assume

$$\left[y^{det}_{i,j,k}|N_{i,j,k}\right] \sim \text{Bernoulli}\left(p^{y}_{i,j,k}N^{1}_{i,j,k}\right), \tag{12}$$

where $N^{1}_{i,j,k} = I_{N_{i,j,k}>0}$ is an indicator variable that zeroes out the detection probability when 0 copies are allocated to a replicate on the logit scale.

Finally, the quantification process, conditioned on detection and the number of copies in a replicate, is

$$\left[\log(y_{i,j,k})|N_{i,j,k}, y^{det}_{i,j,k} = 1\right] \sim \text{Normal}\left(\log(N_{i,j,k}), \sigma^{rep}\right), \tag{13}$$

where $y_{i,j,k}$ is the measured replicate copy number and σ^{rep} is the replicate-level copy number measurement error on the log scale, which could be a function of site, sample, or replicate covariates. Because (1) we condition the quantification process on positive detections and (2) copy number measurements may be censored from below by η_q (Espe et al. 2022), the observed replicate-level quantitative data, $y^{obs}_{i,j,k}$, are:

$$\left[y^{obs}_{i,j,k}|y^{det}_{i,j,k}, y_{i,j,k}\right] = \begin{cases} 0, & \text{if } y^{det}_{i,j,k} = 0, \\ 0, & \text{if } y^{det}_{i,j,k} = 1 \text{ and } y_{i,j,k} < \eta^{q}, \\ y_{i,j,k}, & \text{if } y^{det}_{i,j,k} = 1 \text{ and } y_{i,j,k} > \eta^{q}. \end{cases}$$

This model is depicted in Fig. 1. An important assumption in this quantification process model is that the log copy number measurements are unbiased, i.e., $E[\log(y_{i,j,k})] = \log(N_{i,j,k})$, which can be violated, for example, by a concentration plateau effect (Hunter et al. 2017) or by DNA inhibitors (McKee et al. 2015; Hunter et al. 2019; Sepulveda et al. 2020). We consider the latter in the next section. A final note we will make here is that by conditioning measurement on detection when detection is a function of concentration accounts for the fact that the expected value of measurements for the detected replicates of low concentration samples is larger than $\log(\lambda^{rep}_{i,j})$ because the replicates that are allocated the lowest positive copy numbers are less likely to be detected and thus measureable, and replicates that are allocated 0 copies never produce a quantitative measurement.

4.4 Extended process model: copy inhibition

Here, we consider that the PCR reaction in each replicate may be partially or completely inhibited, which can decrease both the detection probability and the number of copies measured given detection. Compounds found in the environment can inhibit PCR reactions via multiple mechanisms, including binding to the target DNA and binding to or otherwise interfering with reaction products (Opel et al. 2010; McKee et al. 2015). Inhibition is typically identified by comparing

Journal : SmallExtended 10651 | Article No : 632 | Pages : 36 | MS Code : 632 | Dispatch : 13-11-2024

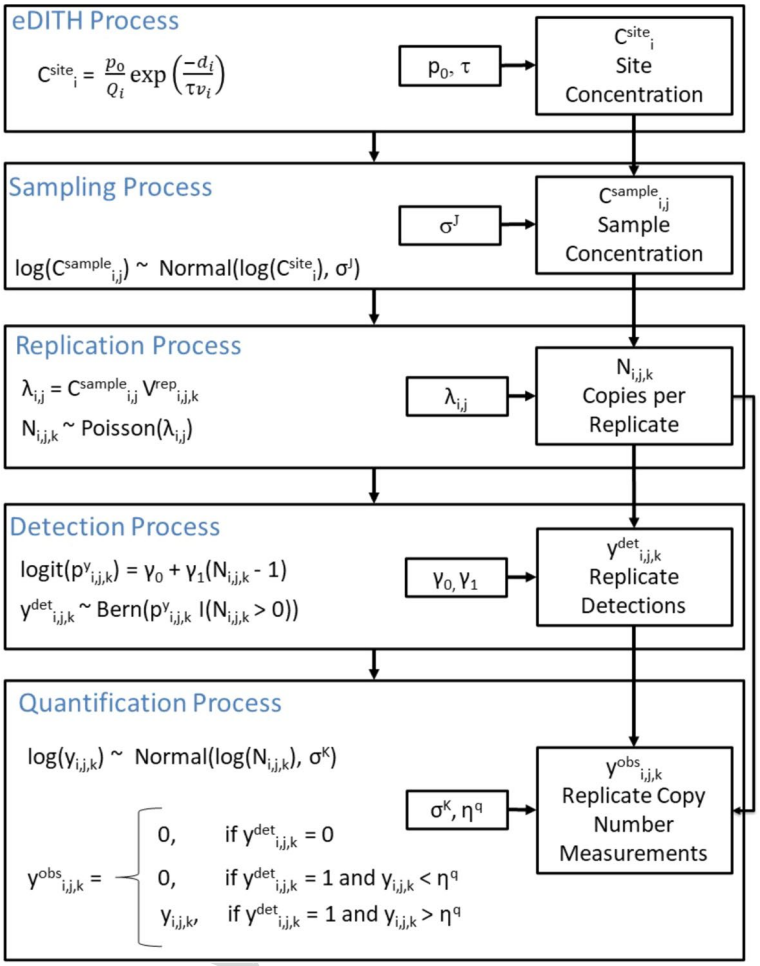

Fig. 1 Model diagram for the exponential removal model without an inhibitor processes. The eDITH process describes how concentration is distributed across sites, the sampling process describes how concentration is distributed across samples at a site, the replication process determines how many copies are allocated to each replicate for each sample, the detection process describes how copies in each replicate are detected, and the quantification process describes how detected copies are measured

the Cq values of IPCs to uninhibited control samples (Volkmann et al. 2007; Jane et al. 2015, see Lab Methods: Inhibition Assessment) and using a deterministic decision rule to exclude samples likely to be inhibited (e.g., samples with a $\Delta Cq \geq 3$ Goldberg et al. 2016), though others have treated ΔCq as continuous measures of inhibition (Volkmann et al. 2007; Lance and Guan 2020). We take the latter approach, modeling the probability of inhibition as a function of replicate copy number, replicate ΔCq, and a sample-level random effect.

For each replicate, the probability of inhibition is $p^{w}_{i,j,k}$, where

Journal : SmallExtended 10651 | Article No : 632 | Pages : 36 | MS Code : 632 | Dispatch : 13-11-2024

$$\text{logit}\left(p^{w}_{i,j,k}\right) = \beta_0 + \beta_1(N_{i,j,k} - 1) + \beta_2 \text{shift}_{i,j,k} + \sigma^{w}\epsilon_{i,j}. \tag{14}$$

$\text{shift}_{i,j,k}$ is the standardized ΔCq covariate, and $\epsilon_{i,j} \sim \text{Normal}(0, 1)$ (non-centered sample-level random effects; Papaspiliopoulos et al. 2007). Note, we expect the $\beta_1 < 0$ and constrain it to be less than zero with a truncated prior (see Supplementary Materials B). The sample random effects account for sample-level heterogeneity in replication inhibition probability, due, at least in part, to sample-level variability in inhibitor concentration. Next, we assume replicate inhibition states are Bernoulli random variables

$$w_{i,j,k} \sim \text{Bernoulli}\left(p^{w}_{i,j,k}\right), \tag{15}$$

with $w_{i,j,k}$ taking value 1 when inhibited and 0 otherwise. If a replicate is inhibited, we assume the copies available to be detected and measured, $N^{thin}_{i,j,k}$, result from a thinning process of the true copy number:

$$\left[N^{thin}_{i,j,k} | N_{i,j,k}\right] \sim \text{Binomial}\left(\theta^{thin}_{i,j,k}, N_{i,j,k}\right), \tag{16}$$

where $\theta^{thin}_{i,j,k}$ is the thinning rate, which could be a function of covariates or random effects. For simplicity, we assume $\text{logit}(\theta^{thin}_{i,j,k}) = \theta_0$. Then, to determine how many copies are available for detection and measurement as a function of the replicate inhibition states, we specify

$$N^{avail}_{i,j,k} = (1 - w_{i,j,k})N_{i,j,k} + w_{i,j,k}N^{thin}_{i,j,k} \tag{17}$$

which evaluates to $N^{thin}_{i,j,k}$ if a replicate is inhibited and $N_{i,j,k}$ otherwise. Finally, we replace $N_{i,j,k}$ with $N^{avail}_{i,j,k}$ in the observation model so that detection and measurement are both conditioned on the inhibition states:

$$\text{logit}(p^{y}_{i,j,k}) = \gamma_0 + \gamma_1(N^{avail}_{i,j,k} - 1), \tag{18}$$

$$\left[\log(y_{i,j,k}) | N^{avail}_{i,j,k}\right] \sim \text{Normal}\left(\log\left(N^{avail}_{i,j,k}\right), \sigma^{rep}\right). \tag{19}$$

Then, the detection model is the same as Eq. (12), except we redefine $N^{1}_{i,j,k} = I_{N^{avail}_{i,j,k} > 0}$, a function of the available copy number instead of the true copy number.

The number of copies available to be detected can be interpreted as the number of copies that inhibitors did not bind to, the number of copies measureable given the magnitude of binding of inhibitors to polymerase in a replicate, or a combination of both factors. More generally, the main feature of the inhibitor model is a large reduction in the detection probability and measured copy number for inhibited samples, which happens regardless of the precise mechanism (Opel et al. 2010; McKee et al. 2015). This extended model is depicted in Supplementary Fig. S1. With this model structure, if a replicate is inhibited, its detection probability and expected log copy number measurement given detection both decrease, with detection probability

decreasing to 0 if no copies are available to be detected. Note that the inhibition states, $w_{i,j,k}$, are not directly observed—we can only observe the effects of inhibition on the copy number detections and measurements. However; the specification of our inhibitor model as part of a larger hierarchical model (Royle and Dorazio 2008) allows the inhibition states to be estimated jointly along with the other model variables and latent states.

4.5 Parameter estimation

We estimated our model parameters using Markov chain Monte Carlo (MCMC) in the Nimble software (Version 1.0.1; de Valpine et al. 2017) in program R (Version 4.0.5; R Core Team 2021). We used Nimble defaults for all MCMC sampler assignments, with some exceptions, specifically, (1) for the inhibitor models, we added user-defined samplers that were required to adequately sample the posterior (described in Supplementary Materials B), (2) due to strong posterior correlation, we used a separate block Metropolis–Hastings updates (Ponisio et al. 2020) for process parameters p_0, θ^{site}, τ or α, detection parameters γ_0 and γ_1, and inhibitor parameters β_0^w and β_1^w. Our priors can be found in Supplementary Materials B.

4.6 Data analysis

4.6.1 Model comparisons

To investigate the evidence for and effects of both a non-constant eDNA removal rate with respect to time and eDNA inhibitors, we fit four models:

- Model I–PL—accounts for inhibitors, power law removal,
- Model I–E—accounts for inhibitors, exponential removal,
- Model N–PL—ignores inhibitors (null), power law removal,
- Model N–E—ignores inhibitors (null), exponential removal.

While the following are not completely conclusive on their own, we suggest that evidence supporting the inhibitor models would be (1) a strong lack of fit when ignoring inhibitors that is reduced when they are modeled (e.g., Model N–PL vs. Model I–PL), (2) a clear negative relationship between the probability of replicate-level undermeasurement events (hypothesized to be caused by inhibition) and the number of copies in a replicate, and (3) a positive relationship between the probability of replicate-level undermeasurement events and the replicate ΔCq.

If the inhibitor models are a good approximation of reality, we expected (by logical implications of the model structure) that when ignoring inhibitors, we would (1) underestimate site concentrations, with larger underestimation as site concentration decreases, (2) overestimate the eDNA removal rate due to under-measuring more at lower concentration sites farther from the source, (3) overestimate both the sampling and measurement variability which must accommodate the effects of inhibition, and (4) underestimate the effect of replicate copy number on detection probability

because the copy number in each replicate will be underestimated, on average. To compare the inhibitor models to the null models, we used posterior predictive checks (Gelman et al. 1996; Conn et al. 2018) and the conditional Watanabe–Akaike Information Criterion (WAIC; Watanabe and Opper 2010; Gelman et al. 2014). For the posterior predictive check, we used the observation model deviance as the discrepancy function (King et al. 2009; Conn et al. 2018). For the null models, the observation model deviance is

$$T(\boldsymbol{y}^{obs}, \boldsymbol{y}^{det}, \boldsymbol{N}, \sigma^{rep}, \gamma_0, \gamma_1) = -2 \log\left([\boldsymbol{y}^{obs}|\boldsymbol{y}^{det}, \sigma^{rep}, \boldsymbol{N}][\boldsymbol{y}^{det}|\gamma_0, \gamma_1, \boldsymbol{N}]\right). \quad (20)$$

The observation model deviance for the inhibitor model is the same as for the null models, except we replace $\boldsymbol{N}$ with $\boldsymbol{N}^{avail}$. For each data point, we computed the Bayesian P-value, the probability each observed data point's discrepancy is more extreme than that of data simulated from the posterior. We considered observations with Bayesian P-values less than 0.05 to be poorly explained by the model and assumed models with more extreme data were less supported.

To compare inhibitor models via WAIC, we used the conditional WAIC (cWAIC) that considers the observation model likelihood conditioned on the number of copies allocated to each replicate, $[\boldsymbol{y}^{obs}|\boldsymbol{y}^{det}, \sigma^{rep}, \boldsymbol{N}][\boldsymbol{y}^{det}|\gamma_0, \gamma_1, \boldsymbol{N}]$. We also used WAIC to compare the removal models; however, cWAIC was not a useful criterion for the process model. In theory, the cWAIC may allow us to compare the exponential and power law process models for these 78 samples (not population-level inference). However, the sample concentrations estimated by these two models were nearly identical (see Results) because the sampling variation was large relative to variation in the observation model, yielding very little shrinkage of sample means toward the site means (for a discussion of shrinkage see Gelman et al. 2013), and thus nearly equivalent conditional likelihoods and WAICs.

While the likelihoods conditioned on the latent variables were nearly identical, the process model likelihood for the distribution of sample means around site means on the log scale, e.g., $[\log(\boldsymbol{C}^{samp})|p_0, \tau, \theta^{site}]$ in the exponential removal model, were not. In this case, marginal WAIC (mWAIC) that also considers the process model likelihood is generally more appropriate for process model selection, and further, it considers the ability of models to predict measurements for new clusters (Merkle et al. 2019; Ariyo et al. 2020, 2022), which here are samples, instead of the 78 samples we did measure (population-level inference). For the exponential model, the marginal likelihood is $[\boldsymbol{y}^{obs}|\boldsymbol{y}^{det}, \sigma^{rep}, p_0, \tau, \theta^{site}][\boldsymbol{y}^{det}|\gamma_0, \gamma_1, p_0, \tau, \theta^{site}]$. With continuous random effects as we have for the sample concentrations, the marginal likelihood needs to be approximated, for example, with importance sampling, which can be computationally costly (Tran et al. 2021). Further, in our model, to approximate this marginal likelihood, we must first integrate out $\boldsymbol{N}^{rep}$, which requires summing over large ranges of integers for every replicate.

For the null models, we were unable to both integrate out $\boldsymbol{N}^{rep}$ and approximate the marginal likelihood in a reasonable amount of time, and for the inhibitor models, we were unable to integrate out $\boldsymbol{N}^{rep}$ in a reasonable amount of time. Therefore, we instead computed sample-level WAIC using the process model likelihood and the posterior modes of the sample log concentrations from the full exponential

Journal : SmallExtended 10651	Article No : 632	Pages : 36	MS Code : 632	Dispatch : 13-11-2024

release models as data, $[\log(\hat{\boldsymbol{C}}^{samp})|p_0, \tau]$. Note, we removed θ^{site} from the marginal likelihood here since we used it to compute the sample log concentrations at the first site to reflect what they were before thinning. We chose to use the sample log concentration point estimates from the exponential model because (1) to compare WAIC, the observed data must be the same, and (2) choosing the exponential estimates a priori favors the exponential model to the degree the sample concentrations are shrunk toward the exponential process model site means. In sum, we pragmatically compared the release models evaluated at our best estimates of the sample concentrations. This approach ignores uncertainty in the sample concentrations, but is arguably more reliable than the common practice of averaging technical replicates to obtain sample concentrations to then use as data and compare models due to the challenges of computing sample means outlined in the Introduction.

4.6.2 Independent eDNA production rate estimate

While the eDNA production rate, p_0, in our experiment was unknown, we used three samples collected from the cooler from which water was released within 15 min of completing the field sample collection and an estimate of the release rate from the cooler (220 mL/min) to produce independent estimates of p_0. Because we could not estimate all the sampling, replication, and observation process parameters with only three samples, and the measured replicate copy numbers from cooler samples were large (5.8–8.4 million), we used a simplified estimation approach. We first estimated the sample log concentrations by averaging the replicate concentrations on the log scale and then used these averages as our three data points. Then, because three data points were not sufficient to estimate the sampling standard deviation with acceptable precision, we did a sensitivity analysis where we estimated p_0 from the cooler samples assuming σ^{samp} was 0.25, 0.5, 1.0, or 1.5, where 0.25 and 0.5 were lower than what we estimated from the inhibitor release models and 1.5 was higher. We then compared the visual overlap in the posterior distributions of p_0 from the four release models to these hypothetical sampling standard deviations for the cooler models.

4.6.3 MCMC details

For each of the 4 release models, we ran 3 MCMC chains for 300,000 iterations each, with model parameters and latent variables thinned by 25 and 250 iterations, respectively. We discarded 25,000 pre-thinned iterations and assessed convergence using the Gelman–Rubin Statistic (Brooks and Gelman 1998) ensuring the 95% CI upper bound was less than 1.1 for all parameters. Posterior modes were used as point estimates and 95% highest posterior density (HPD) intervals were used as interval estimates. Because the posteriors for $\boldsymbol{N}$, $\boldsymbol{N}^{thin}$, $\boldsymbol{N}^{avail}$, and $\boldsymbol{C}^{sample}$ were often multimodal in the inhibitor models, we used the HDinterval R package (Meredith and Kruschke 2020) to produce discontinuous HPD intervals. For each of the cooler models (each level of σ^{samp}), we ran 1 chain for 25,000 iterations, discarding the first 5000 iterations.

Journal : SmallExtended 10651	Article No : 632	Pages : 36	MS Code : 632	Dispatch : 13-11-2024

4.7 Simulation study

We conducted a simulation study to characterize how well parameters of each model were estimated in terms of percent relative bias (absolute bias divided by the true parameter value and then multiplied by 100), 95% coverage (proportion of data sets for which the 95% HPD covers the true parameter value), and the coefficient of variation (CV; posterior standard deviation divided by posterior mode multiplied by 100) when using data similar to ours in terms of the data dimensions, hydrology, and parameter values. We simulated 100 data sets from each of four models using the parameter estimates from the field data, with the same number of sites, site distances, replicate number, and hydrological parameters. The simulation scenarios differed from the field data models in two ways—we excluded the thinning process at the first site due to the "plume effect" to assess how well the eDNA production rate, p_0, can be estimated when ignoring this nuisance parameter, and we excluded the ΔCq covariate as it may not always be available.

For each simulated data set from the null and inhibitor models, we ran 3 MCMC chains for 150,000 and 300,000 iterations, respectively, and thinned posteriors by 25 to reduce file sizes. For null and inhibitor models, we discarded a minimum burn in of 5000 and 35,000 pre-thinned iterations, respectively. After discarding this burn in, we computed the Gelman–Rubin statistic ($\hat{R}$; Gelman and Rubin 1992) for each parameter, ensuring that the 95% confidence interval upper bound of the statistic was below 1.1. For posteriors with $\hat{R}$ 95% confidence intervals greater than 1.1 for any parameter, we discarded more burn in after visual inspection to meet this condition. For point estimates, we used the posterior mode, and for interval estimates, we used the 95% HPD interval. For each data set, we computed the CV for all parameters by dividing the posterior standard deviation by the absolute value of the posterior mode and multiplying by 100. We report the CV averaged across data sets for each model. One exception was for β_0^w, which had point estimates very close to zero, leading to large CVs which were not informative of parameter precision (Kvålseth 2017). For this parameter, we computed the CV as the averaged standard deviation divided by the averaged posterior mode multiplied by 100.

5 Results

5.1 Observed data and inhibition assessment

We observed no amplification in negative controls or in samples collected upstream of the introduction point and positive controls amplified as expected. The replicate-level quantitative data ranged from 2.22 to 5.91 $\log_{10}$ copies/L and 0.22–3.91 $\log_{10}$ copies per reaction (Supplementary Fig. S2a). We observed 24 replicates (out of 390) that failed to detect eDNA, with 1, 5, 7, 1, 2 and 8 failed detections at distances of 0.5, 40, 300, 400, 500, and 1000 m, respectively. Three samples failed to detect eDNA across all five replicates, one sample each at distances of 40, 300, and 1000

Journal : SmallExtended 10651 | Article No : 632 | Pages : 36 | MS Code : 632 | Dispatch : 13-11-2024

m. Our inhibition assessment did not indicate inhibition for any replicates using the decision rule of $\Delta Cq \geq 3$. Shifts in Cq ranged from -0.13 to 1.60 with a mean of 0.11 cycles. The distribution of ΔCq was right skewed, with most values clustered slightly above zero (Supplementary Fig. S2b).

5.2 Analysis of field data

The four models we considered produced substantially different parameter estimates, leading to different inferences about the ecological and observational processes that produced our data (Table 1). The inhibitor models estimated that the sampling process standard deviation, σ^{samp} was smaller and the quantification process standard deviation, σ^{rep} was larger, compared to the null models. The inhibitor models further estimated that the removal rate (governed by α or τ) was lower compared to the null models, and that site concentrations were higher, particularly at the sites farthest from the source (Fig. 2).

The power law removal models estimated the eDNA production rate at the source to be much larger than the exponential removal models (Fig. 3) and correspondingly, estimated the percent of total concentration that is measurable at the first site, θ^{site} to be lower (Table 1). Finally, the effect size of replicate copy number on replicate detection probability was estimated to be greater in the inhibitor models relative to the null models.

The Bayesian P-values from the deviance discrepancy function identified 14 samples as having replicates that were more extreme than expected under both versions of the null models (Table 2). These samples were characterized by having lower copy numbers, with one or more replicate measurements being much larger than the others, and they disproportionately came from the sites with the lowest measurable concentrations (first site with plume effect and sites farthest from the source). For the inhibitor models, the Bayesian P-values identified four samples having replicate measurements that were more extreme than expected by the model. The replicates of these samples were also imbalanced but to a lesser or greater degree than expected compared to our thinning rate estimate, $\text{inv.logit}(\theta_0) = 0.09$, suggesting heterogeneity in the sample-level thinning rate. WAIC favored the inhibitor models over the null models, with the increased number of effective parameters outweighed by the substantially higher log posterior predictive density (Table 3).

Our WAIC estimates using the likelihood for sample log concentrations (Table 3) favored the power law model over the exponential model by 28.27 and 37.46 units when considering and not considering inhibition, respectively. The similarity of the posterior modes for log sample concentrations between removal models can be visualized in Supplementary Fig. S3, where estimates from the null models are nearly identical between exponential and power law removal, and estimates from the inhibitor models were nearly identical except for 2–3 data points. We provide this information to justify using the posterior modes of sample log concentrations from the exponential model as data to evaluate the relative support for each release model, and reiterate that doing so a priori favors the exponential model to the extent that the posterior modes for log sample concentrations differ between removal models. Our

Journal : SmallExtended 10651 | Article No : 632 | Pages : 36 | MS Code : 632 | Dispatch : 13-11-2024

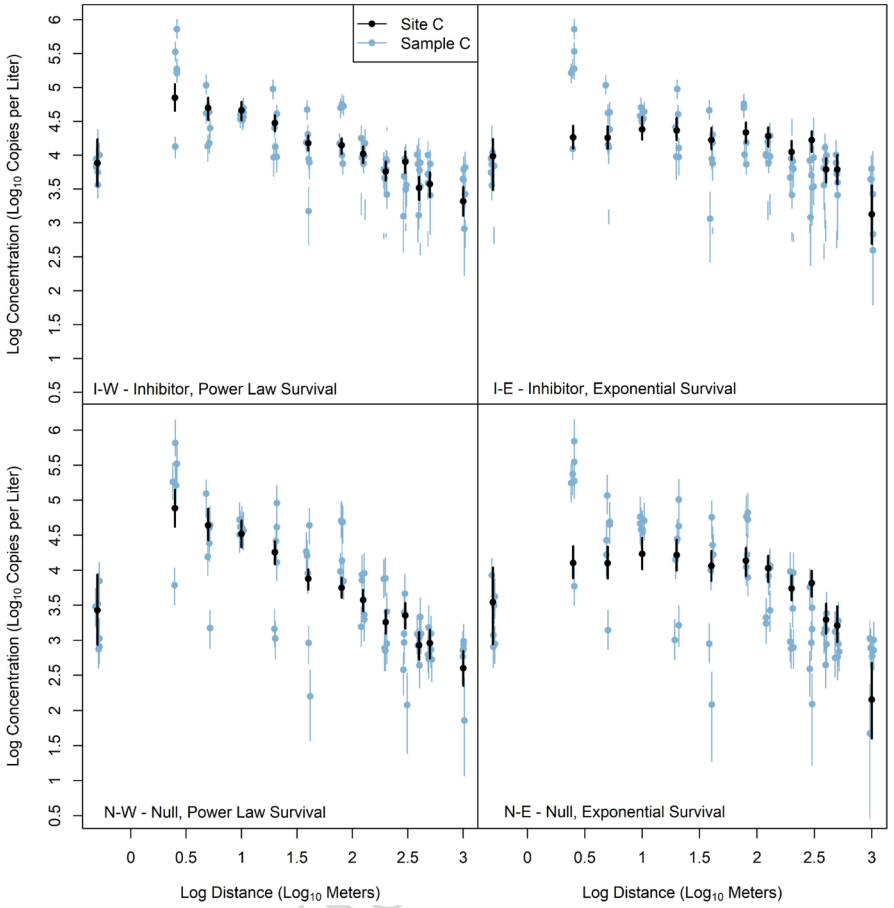

Fig. 2 Posterior point and interval estimates of site and sample concentration as a function of distance for all four models. Note, some 95% HPD intervals are discontinuous due to multimodal posterior distributions. Estimates from Models I–PL and I–E accounting for inhibitors are generally higher, and to a greater magnitude as distance increases. Estimates from Models I–PL and N–PL are higher at sites 2–4 compared to Models I–PL and N–PL, respectively, due to an increasing removal rate through time

second line of evidence to discriminate between removal models is the comparison of the posteriors for the eDNA production rate, p_0, between the release and cooler models (Fig. 4). While we do not know what the sampling standard deviation, σ^{samp}, was in the cooler, the p_0 estimates from all cooler models overlap more with the power law release models, particularly when inhibition is considered. Our point estimate for σ^{samp} was 0.15; however, this estimate is unlikely to be accurate with only 3 samples.

Parameter estimates with posterior standard deviations and 95% HPD intervals for Model I–PL can be found in Table 4. Model I–PL estimated that many replicates in the range of 1.5–2.5 $\log_{10}$ copies were substantially undermeasured, but after accounting for the inhibition process, the copies available to be measured

Journal : SmallExtended 10651 | Article No : 632 | Pages : 36 | MS Code : 632 | Dispatch : 13-11-2024

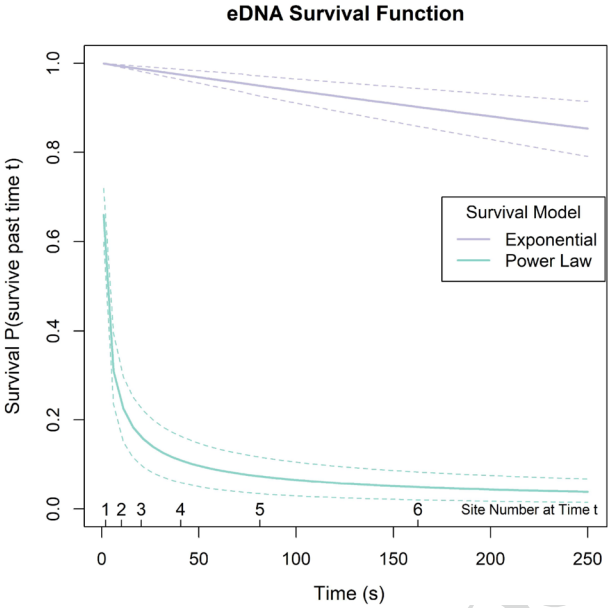

Fig. 3 Survival functions from Models I–PL and I–E, with power law and exponential survival, respectively. Under the power law model, there is more eDNA estimated to be added at the source location relative to the exponential, and faster removal that slows down through time. The expected time at which eDNA reaches sites 1–6 are indicated on the plots, which were derived from our mean velocity measurement

corresponded well with the measured copy numbers (Fig. 5). In Model I–PL, the probability of inhibition was estimated to be inv.logit($\hat{\beta}_0^w$) = 0.85 for a replicate with 1 copy (and random effect value set to 0), with a negligible probability of inhibition over 300 copies/replicate (Fig. 6). The ΔCq covariate was estimated to be positively-related to the probability of inhibition (Table 4), with a 95% HPD that did not overlap 0 and a posterior probability of being greater than 0 equal to 0.99.

5.3 Simulation study A

Our ability to estimate parameters in terms of bias, coverage, and precision (CV) varied across parameters and models, with generally better estimates from null models over inhibitor models and exponential over power law removal models (Supplementary Table S1). For the null models, coverage was roughly nominal (e.g., 95% CI covered the true value 95% of the time), but the detection parameters were moderately biased (−7.2 to 24.6%) and estimated imprecisely (CVs of 58.8–133.8%). Further, the null model with exponential removal estimated the eDNA production rate, p_0 with minimal bias (2.8%) and a CV of 29.0%, whereas the estimate from the null power law removal model was positively biased by 5.2%, and less precise (CV of 56.6%). The sampling and measurement standard deviations, σ^{samp} and σ^{rep}, were estimated with minimal bias (< 3%) in the null models.

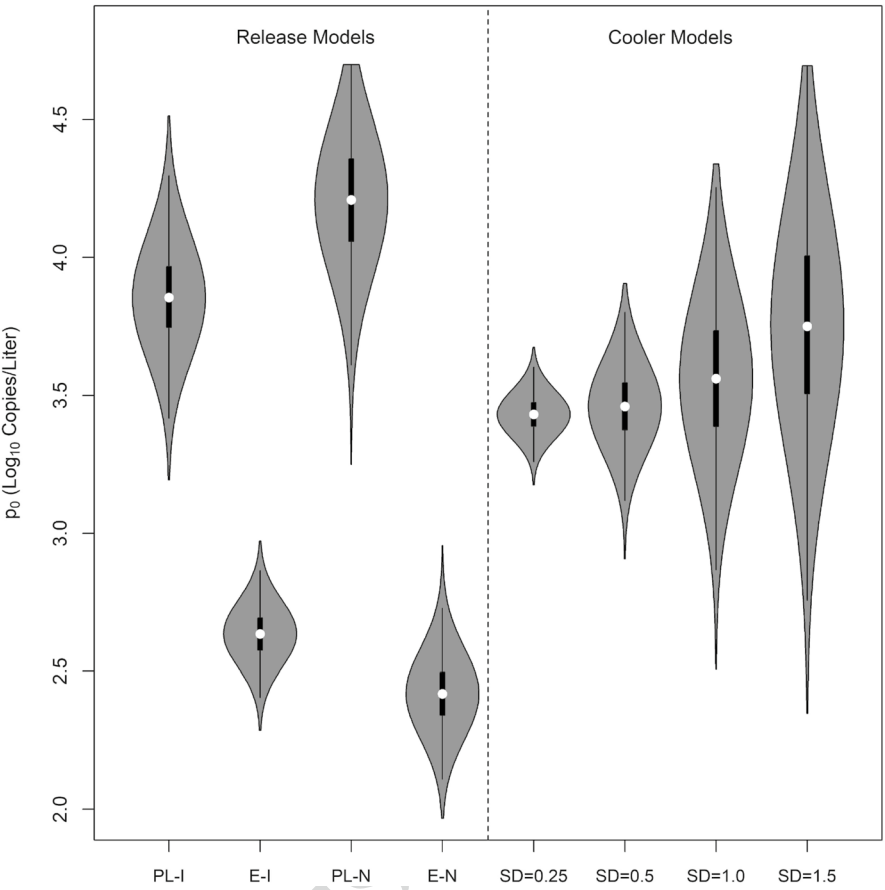

Fig. 4 Plots of the posterior distributions of the eDNA production rate, p_0, from the four release models and four cooler models with different hypothetical sampling standard deviations, σ^{samp} (indicated with "SD" on the plot). For release models, "PL" indicates "power law," "E" indicates "exponential," "I" indicates "inhibitor," and 'N" indicates "null." More overlap between particular release and cooler models indicates more consistency between the estimates

For the inhibitor models, we saw results similar to the null models. Overall, coverage was roughly nominal for the inhibitor models with the possible exception of reduced coverage for some parameters in model I–PL (our estimates are subject to some sampling variability with only 100 data sets). The detection parameters were biased (−10.6 to 2.0%) and estimated imprecisely (CVs of 52.9–93.6%). The eDNA production rate, p_0, was estimated with modest negative bias in Model I–E with exponential removal (−4.6%) and modest positive bias in model I–PL with power law removal (8.6%). The p_0 estimates in the inhibitor models were more precise as judged by the CV, likely due to the larger simulated values used in the inhibitor models leading to larger posterior modes. All parameters determining the probability of inhibition were estimated with bias, particularly the intercept β_0^w, which was

Journal : SmallExtended 10651 | Article No : 632 | Pages : 36 | MS Code : 632 | Dispatch : 13-11-2024

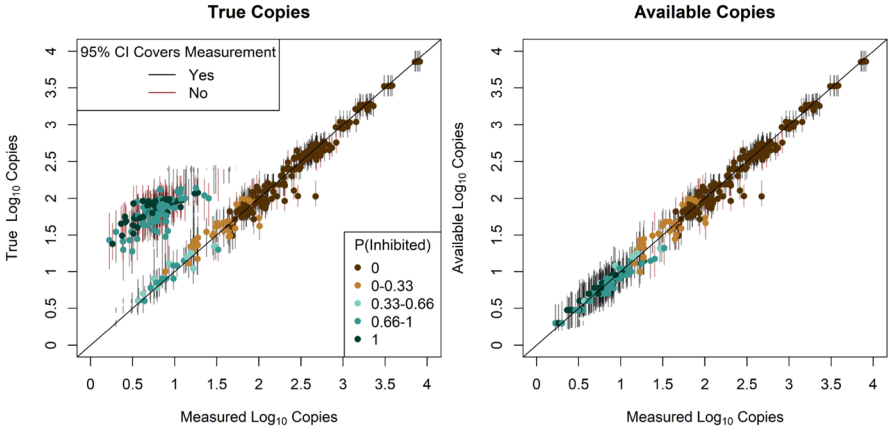

Fig. 5 Comparison of the relationship between measured and true copies in each replicate (left) and measured and available copies in each replicate (right) from Model I–PL accounting for inhibitors. In each plot, the posterior probability of inhibition is indicated by the color of the point estimate and 95% HPD intervals are depicted, some of which are discontinuous due to multimodal posteriors. In the plot on the left, the group of true copies measured too low with poor coverage correspond to the samples to which the model assigns a high posterior probability of inhibition. After accounting for inhibition (plot on right), the relationship between measured and available copies is roughly linear with coverage 0.87

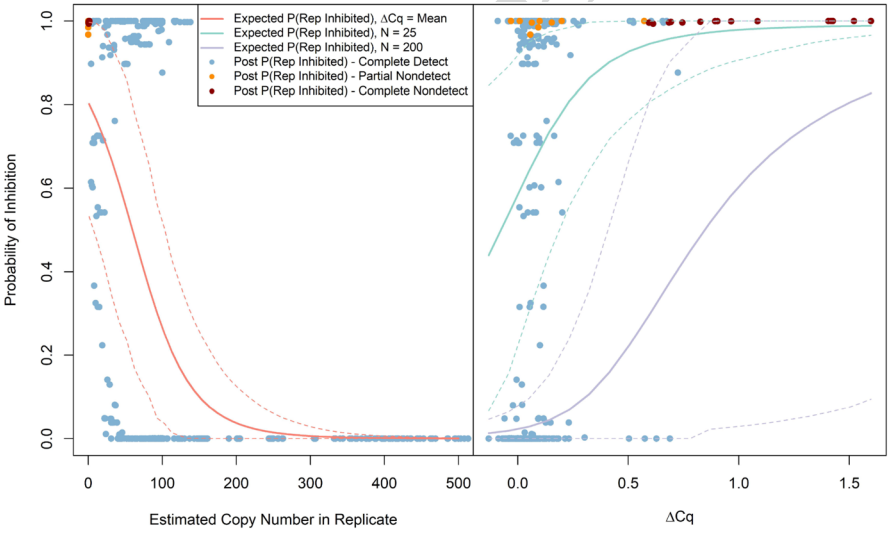

Fig. 6 Plots depicting the effects of copy number and ΔCq on the expected probability of inhibition (posterior mean and 95% HPDs), $p^{w}_{i,j,k}$, and the posterior probability of inhibition, $P(w_{i,j,k} = 1)$. Replicates from samples with no detections (complete nondetects) are colored red, and replicates without detections in samples where other replicates were detected (partial nondetects) are colored orange. The probability of inhibition declines as a function of replicate copy number, with complete and partial nondetects all being estimated to have very few copies (left). The probability of inhibition increases with ΔCq, particularly for replicates with fewer copies (N = 25 scenario)

Journal : SmallExtended 10651 | Article No : 632 | Pages : 36 | MS Code : 632 | Dispatch : 13-11-2024

Table 1 Parameter point estimates for all four models applied to the field data

Process	Par	Models			
		I–PL	I–E	N–PL	N–E
eDITH	p_0	6134.78	419.13	12, 076.28	244.69
eDITH	α	0.59	.	0.91	.
eDITH	τ	.	1431.82	.	873.94
eDITH	θ^{site}	0.04	0.34	0.01	0.15
Sampling	σ^{samp}	0.90	1.20	1.34	1.67
Replicate Inhibition	β_0^w	1.44	1.46	.	.
Replicate Inhibition	β_1^w	− 0.02	− 0.02	.	.
Replicate Inhibition	β_2^w	1.16	1.19	.	.
Replicate Inhibition	σ^w	3.28	3.44	.	.
Inhibitor Thinning	θ_0	−2.31	−2.36	.	.
Detection	γ_0	− 2.52	− 2.41	− 2.31	− 2.25
Detection	γ_1	2.80	2.79	1.28	1.32
Quantification	σ^{rep}	0.29	0.29	0.68	0.68

Model I–PL accommodates inhibitors and has power law removal, Model I–E accommodates inhibitors and has exponential removal, Model N–PL does not accommodate inhibitors and has power law removal, Model N–E does not accommodate inhibitors and has exponential removal. p_0 was modeled in m^3/s units and presented here in L/s units

negatively biased by 19.7–23.3% in the inhibitor models. As in the null models, the sampling and measurement standard deviations, σ^{samp} and σ^{rep}, were estimated with minimal bias (<3%), except for σ^{samp} in model I–PL with a bias of 5.9%.

6 Discussion

We developed a hierarchical model for eDNA fate and transport experiments that accommodates more mechanistic detail about how eDNA is detected and measured than existing models. We also conducted an eDNA release experiment to demonstrate the utility of this modeling approach for estimating eDNA removal parameters in the presence of ecological and measurement variability. Two distinctive features of the model are that site concentrations are modeled as the product of an eDNA removal process as a function of time (using the eDITH approach of Carraro et al. 2018) and that replicate copy numbers are regarded as latent variables modeled with a count distribution. The latter feature has several advantages for low concentration samples and facilitates modeling detection, measurement error, and sources of bias as functions of the ecological quantity being measured—the discrete number of copies in each replicate. Using this model, we were able to provide evidence that the eDNA removal rate in our experiment declined through time (e.g., power law removal) and that the allocation of measurable copies across replicates was overdispersed relative to the Poisson in a subset of samples. We then developed a model for

Journal : SmallExtended 10651 | Article No : 632 | Pages : 36 | MS Code : 632 | Dispatch : 13-11-2024

Table 2 Samples with replicates where Bayesian P-values from posterior predictive checks indicated lack of fit, defined as the P-value being less than 0.05

Model	Site	Sample	Rep 1	Rep 2	Rep 3	Rep 4	Rep 5
Null	1	1	2.57	66.33	62.70	3.41	3.86
Null	1	3	0	7.08	4.88	472.19	4.16
Null	1	6	125.24	71.73	4.75	121.01	5.86
Null	8	5	62.79	6.35	164.17	11.97	8.67
Null	10	1	110.24	5.66	9.56	7.31	5.53
Null	11	3	8.16	74.08	7.98	10.39	141.60
Null	11	4	68.67	7.37	7.88	11.77	6.02
Null	11	6	70.95	2.56	3.30	84.97	4.21
Null	12	1	2.31	7.94	5.57	2.64	52.09
Null	12	2	8.30	9.61	4.28	66.94	9.94
Null	12	3	42.74	5.61	0	3.24	2.38
Null	13	3	2.42	48.81	18.51	1.83	0
Null	13	4	31.04	3.61	0	87.01	4.80
Null	13	5	70.73	3.49	5.00	8.21	5.42
Inhibit	1	3	0	7.08	4.88	472.19	4.16
Inhibit	1	4	44.27	102.19	38.40	16.92	18.84
Inhibit	6	4	202.90	54.30	62.58	90.22	77.76
Inhibit	8	4	67.78	74.98	76.75	291.60	76.44

Samples are listed by model ("Null" and "Inhibit" without and with modeling inhibitors, respectively), site, and sample, along with the observed data for each sample replicate. Null models are N–E and N–PL and inhibitor models are I–E and I–PL

Table 3 WAIC table showing the WAIC, log posterior predictive density (lppd) and effective number of parameters (pWAIC) for all four models

Model	WAIC Target	WAIC	lppd	pWAIC
I–PL	Rep	334.96	− 33.61	133.87
I–E	Rep	333.34	− 33.16	133.51
N–PL	Rep	912.28	− 360.87	95.27
N–E	Rep	913.20	− 360.33	96.27
I–PL	Samp	219.15	− 105.75	3.83
I–E	Samp	256.61	− 124.49	3.82
N–PL	Samp	278.84	− 135.26	4.16
N–E	Samp	307.11	− 149.87	3.69

Two types of WAIC are used, with a WAIC Target of "Rep" being the conditional WAIC at the level of replicates and a WAIC Target of "Samp" being the conditional WAIC at the level of samples. For sample-level WAIC, we were unable to incorporate the uncertainty in the sample concentrations, and the sample-level WAIC values are not directly comparable between the null and inhibitor models, see "Methods"

Journal : SmallExtended 10651 | Article No : 632 | Pages : 36 | MS Code : 632 | Dispatch : 13-11-2024

Table 4 Parameter point and interval estimates and posterior standard deviations from Model I–PL that accommodates inhibitors and considers power law removal

Process	Par	Est	SD	Lower	Upper
eDITH	p_0	6134.78	3079.41	2834.56	13, 769.82
eDITH	α	0.59	0.07	0.47	0.74
eDITH	θ^{site}	0.04	0.03	0.01	0.12
Sampling	σ^{samp}	0.90	0.10	0.75	1.13
Replicate Inhibition	β_0^w	1.44	0.98	− 0.24	3.65
Replicate Inhibition	β_1^w	− 0.02	0.01	−0.05	− 0.01
Replicate Inhibition	β_2^w	1.16	0.54	0.20	2.32
Replicate Inhibition	σ^w	3.28	0.77	2.20	5.10
Inhibitor Thinning	θ_0	− 2.31	0.10	− 2.51	− 2.11
Detection	γ_0	− 2.52	1.28	− 5.63	− 0.70
Detection	γ_1	2.80	1.78	1.05	6.99
Quantification	σ^{rep}	0.29	0.02	0.26	0.33

p_0 was modeled in m^3/s units and presented here in L/s units

how eDNA inhibitors might reduce the measurable copy numbers in the replicates and show the pattern of overdispersion in our observed data is largely consistent with this model.

Treating copy numbers in replicates as count random variables provides several advantages when site and sample concentrations are low. To date, quantitative eDNA analyses have typically assumed sample or replicate concentrations are normally-distributed, usually on the log scale (Carraro et al. 2018; Espe et al. 2022; Shelton et al. 2019). Our model highlights that replicate-level measurement error is the product of both sampling variation when allocating copies to the replicates (Dube et al. 2008; Lesperance et al. 2021) and the measurement error conditioned on the number of copies in each replicate (due to variation in factors such as reading fractional cycle numbers; Shelton et al. 2019). An implication of a count model for the replication process is that a normal approximation will be a less appropriate when measuring small copy numbers (Espe et al. 2022) that are typical of many eDNA applications. Then, when sample concentrations are low enough that qPCR replicate-level zeros are observed, it is unknown whether a zero is observed because there were no target DNA copies allocated to a replicate or because the allocated copies were undetected (Dube et al. 2008; Lesperance et al. 2021). To compute an unbiased sample mean concentration in the presence of observed zeros, the replication process zeros need to be included, as do the true allocated copy numbers for replicates with failed detections, which are not observed.

Techniques that allow a probabilistic interpretation of zeros and non-detections have been recognized as critical by many disciplines, like analytical chemistry and public health (e.g., Chik et al. 2018), and have been used by eDNA practitioners when computing the limit of detection in qPCR (Dube et al. 2008; Lesperance et al. 2021). By conditioning detection on copies being present in replicates, and relating the detection probability to the number of copies in a replicate, our model can

Journal : SmallExtended 10651	Article No : 632	Pages : 36	MS Code : 632	Dispatch : 13-11-2024

probabilistically resolve these sources of zeros and produce less biased estimates of replicate copy numbers and sample concentrations in this situation. In practice, the accuracy of the resulting estimates will depend on how well model assumptions are met, and estimates may be very imprecise when samples have concentrations so low that most replicates are true sampling zeros. Further, in Simulation Study A, we show that the detection parameters that are a function of latent copy numbers are weakly identifiable, estimated with low precision and moderate bias. We assume this is due to the magnitude of uncertainty in the estimates of the latent copy numbers near zero, which is greater in the inhibitor models where the bias in the detection probability of one copy is larger. Therefore, the performance of this model in terms of bias and precision of the ecological parameters in scenarios with lower sample concentrations than we observed and/or greater sampling variability should be further investigated. This approach of partitioning variation between the allocation of copies and measurement of copies may also be used in standard curve experiments (e.g., Klymus et al. 2020) to relate Cq to the realized, instead of expected, copy number of standards. Doing so could reduce the nonlinearity seen in standard curve calibration regressions (Klymus et al. 2020) due to observing true and false zeros at low concentration standards.

Including latent replicate copy numbers in the model also provides a means for detecting deviations from Poisson variability in the replication process, and exploring hypotheses about potential causes of this assumption violation. We were able to use posterior predictive checks to identify lack of fit in our null models consistent with overdispersion in the number of copies allocated to replicates. This overdispersion was only seen in a subset of samples, and appeared stochastic in nature, with replicates tending to show a bimodal pattern of high and low measurements in affected samples. In theory, general overdispersion could result from sample-level variability in measurement error, given the number of copies allocated to each replicate, but we were unable to devise a measurement error hypothesis that explained sample-level heterogeneity and the apparent bimodality in affected samples. Further, we did not find general overdispersion hypotheses, such as pipetting error, to be plausible because most samples were consistent with Poisson replication process variability.

A benefit of our hierarchical modeling approach is that we can construct and evaluate hypotheses for plausible mechanisms of this overdispersion pattern. Using the common decision rule of $\Delta Cq \geq 3$ (e.g., Hartman et al. 2005; McKee et al. 2015; Goldberg et al. 2016), none of our samples would be classified as inhibited (Fig. S2b). However, given the general vulnerability of PCR quantification to inhibition (Opel et al. 2010; Sidstedt et al. 2020), the lack of a standard criterion to describe degrees of inhibition (Lance and Guan 2020), and variation in how different assays respond to the same inhibitor (Lance and Guan 2020), we suspected this decision rule may not be well calibrated for our assays and inhibition may have gone undetected using this method. We used our extended hierarchical model to evaluate the hypothesis that eDNA inhibitors were reducing detection probability and measured copy numbers in our field data, and these inhibitor effects were stochastic, leading to undermeasurement of some replicates of some samples. In the model, inhibitors have a continuous effect, causing undermeasurement, then failed detection,

Journal : SmallExtended 10651	Article No : 632	Pages : 36	MS Code : 632	Dispatch : 13-11-2024

depending both on the starting copy number and the magnitude of the underestimation caused by the inhibitors.

We suggest that the posterior predictive checks provide support for the inhibitor models over the null models. The inhibitor model did not provide a clear indication of lack of fit for 13/14 of the poorly explained samples from the null model (Table 2), and the four samples that were identified by the posterior predictive check as indicating lack of fit in the inhibitor model were cases that are consistent with inhibition, but with a thinning rate lower or larger than our estimate of $\theta^{thin} = 0.09$ (assuming binomial variability). This extra-binomial variability could be accommodated with a sample-level random effect in the inhibitor thinning process, or perhaps both the probability and magnitude of inhibition could be related to the same latent variable representing inhibitor concentration in a sample. Conditional WAIC also highly favored the inhibitor model. A second line of evidence for the inhibitor hypothesis is that the probability of inhibition was positively associated with the ΔCq covariate with a posterior probability $\beta_2^w > 0 = 0.99$. Still, we cannot conclusively rule out other causes of the overdispersion we saw in our data, and it may result from more than one cause.

Hypothetically interpreting our field data in light of the inhibitor model, inhibition started to occur in the range of 100–400 copies/replicate. As copy number approached zero, between 60 and 100% of the replicates were likely to be inhibited (interpreting 95% CIs in Fig. 6). If inhibitors were as prevalent in our data as our model suggests, this would indicate that exogenous IPC Cq shifts may not always have high statistical power to detect inhibition at magnitudes that substantially affect measurements. Whether the source of overdispersion we detected was due to a mechanism increasing variability or one causing systematic undermeasurement, like inhibitors, is of high importance. The latter will cause us to systematically underestimate site and sample concentrations disproportionately such that as concentration declines, the rate of eDNA removal is overestimated and the sampling process variability is inflated (i.e., attributing inhibitor-induced variability to ecological variability). Our model provides a framework to compare alternative hypotheses, using either field or experimentally manipulated samples, to such extent that these hypotheses imply that different data will be observed. A final caveat is that the signal of inhibition is eroded as copy number approaches zero because of the magnitude of measurement error given the available copy number. For the inhibitor model parameters to be identifiable, we require samples with concentrations high enough that the magnitude of imbalance (relative to Poisson sampling variability) across replicates is large relative to measurement error, but not so large that inhibition did not occur. Lower concentration samples are more likely to have all replicates inhibited, so no imbalance is observable. Our simulation results indicate that the probability of inhibition parameters ($\boldsymbol{\beta}^w$ and σ^w) were weakly identifiable for data sets similar to ours, and we expect they will be completely unidentifiable in many cases.

By using the eDITH model to describe eDNA removal as a function of time, we were able to provide evidence that the eDNA removal rate was not constant through time. WAIC favored the power law removal model both when we did and did not consider inhibition. Further, the posteriors for p_0 from the power law release model overlapped more with the posteriors for p_0 estimated in the cooler;

Journal : SmallExtended 10651 | Article No : 632 | Pages : 36 | MS Code : 632 | Dispatch : 13-11-2024

however, our cooler estimates are speculative since we do not know the sampling variation in the cooler. Presumably, the turbidity of the stream could increase the sampling standard deviation and our point estimate of the sampling standard deviation in the cooler was 0.15, much lower than estimated in the release models; however, other factors likely need to be considered and the cooler standard deviation was estimated with only three samples. If the power law model is closer to the truth, the eDNA production rate parameter, p_0, is challenging to estimate given our study design and the magnitude of sampling variance we encountered. In Simulation Study A, we see that p_0 is estimated with negligible bias in the exponential removal models, but moderate positive bias in the power law removal models. Then, the CV is roughly twice as large for the power law removal models. We attribute this to the challenge of (1) extrapolating the pattern in observed concentrations back to the source location when concentration is declining rapidly (Fig. 3) and (2) a large sampling standard deviation. We believe these challenges also extend to the more appropriate Weibull removal model, where we found that p_0 and the Weibull scale parameter were effectively jointly unidentifiable with our data, but identifiable if we simulated similar data with a far lower sampling standard deviation. Regardless of the true removal model, using the exponential model if the removal rate decreases through time will negatively bias the estimated eDNA production rate at the source, which will be propagated to downstream metrics like site abundance.

One factor that introduces some unaccounted for uncertainty to our evidence for a declining removal rate is that we do not know the reason that the concentration at the first site was estimated to be lower than the second site. If the mechanism(s) causing the concentration at the first site to be undermeasured causes the concentration at the second site to be overmeasured, this could cause the data to appear to be undergoing a declining rate of removal. Conversely, if this mechanism caused the concentration at sites beyond the first site to also be undermeasured, we would have underestimated the support for the power law removal model over the exponential. Our hypothesis is that concentration at the first site was undermeasured because eDNA did not immediately dissolve throughout the water column (Wood et al. 2020, 2021), and the bucket we used to collect water to then split into the six samples at the first site disproportionately sampled water where the eDNA concentration was lower than average for that site. Our release mechanism deposited water from the cooler on top of the stream and we expect it took some time for the eDNA to reach lower in the water column due to gravitational settling (Harrison et al. 2019). This effect has been documented along the horizontal dimension in rivers (Wood et al. 2020, 2021; Laporte et al. 2020), where it has been termed a "plume effect." We suggest a similar pattern may occur in the vertical dimension when sampling very close to an eDNA source, depending on where in the water column water is sampled. When we sampled the first site, the water with the highest concentration of eDNA may have flowed over the bucket and we may have disproportionately sampled water with a lower concentration of eDNA. If this was the mechanism causing underestimation at the first site, we do not believe it would cause overestimation at the second site. Therefore, we suggest that while not conclusive, our study adds to the evidence for the hypothesis that, in the context of a mass-balance model of

eDNA production, transport, and decay, the removal term is large and the transport term is small (Tillotson et al. 2018).

Finally, we discuss implications of our model and results for applications of the eDITH model to observational data and for occupancy analyses using detection data only. To our knowledge, the eDITH model has only been applied to observational data sets where: (1) the concentration observed at one site is the product of multiple upstream sites with different eDNA production rates and (2) release locations are estimated because they are not known. In contrast, our study system used a single, known release location. If eDNA decay declines at the rate we estimated, the majority of the total eDNA produced in a river network would be ignored, and the resulting site concentrations would be underestimated. Further, this underestimation would be predominately close to the sources, so measured site concentrations would not be related to true site concentrations by the same proportionality constant across space (inhibition could also cause deviations from a fixed proportionality constant). The assumptions of the eDITH model are hard to scrutinize given the number and magnitude of sources of ecological and measurement variability and the number of parameters and latent variables that must be estimated. We demonstrated how some assumptions can be better tested in more simple experiments and recommend more and better-controlled experiments be conducted in order to better understand the reliability of this approach when applied at large spatial scales.

While we developed our model in the context of an eDNA release experiment with a single source, eDNA production at a site can be conditioned on latent occupancy states. This model can also be used for occupancy-type designs with independent sites, with site concentration conditioned on latent occupancy states. A principal implication of our model for natural resource management is that for occupancy analyses, site, sample, and replicate variability in concentration and copy number induce detection heterogeneity at all three of these levels. If this variability is not modeled using either observed covariates or random effects, ecological inference may be unreliable. Perhaps the most important effect is that if (1) sites vary in concentration and (2) at least some site concentrations are low enough to lead to missed detections, there will be site heterogeneity in detection probability and subsequent underestimation of the occupancy probability, and thus the potential for misguided natural resource decision making (Royle and Nichols 2003). Also of importance is that the reliability of inference from false positive occupancy models depends on how well heterogeneity in true positive detection is accounted for (McClintock et al. 2010; Ferguson et al. 2015).

Replacing our eDITH process with processes for independent site occupancy and concentration conditioned on site occupancy would allow for the occupancy states and concentrations at unmeasured sites to be jointly estimated. A caveat, though, is that the reliability of the concentration estimates at sites with no detections (disproportionately those with the lowest concentrations) will likely depend on the adequacy of the distribution used to model site concentration variability (e.g., log-normal variability in site concentration). Further, the performance of such a model will depend on the abundance and reliability of copy number data. Even if not used in practice for occupancy analyses, our model can be used to assess how reliable ecological inference is in the presence of these forms of detection heterogeneity.

Ultimately, biostatistical approaches such as those presented in this study help resolve uncertainties associated with eDNA fate and transport as well as qPCR detection and measurement of scarce molecules. Implementation of these types of approaches is needed to more fully take advantage of the potential for eDNA analysis to contribute natural resource management (Kelly et al. 2023).

Appendix: Lab methods and selected results

Methods: assay development

Assays designed for eDNA studies using qPCR generally target short amplicons that are between 50 and 150 base pairs (bp) in length (Goldberg et al. 2016; Rees et al. 2014) because PCR efficiencies are higher for shorter amplicons (Bustin and Hugget 2017) and because shorter DNA fragments tend to be more available for detection in aquatic environments than longer fragments (Bylemans et al. 2018). To explore differences in transport dynamics of short and long DNA fragments, two probe-based qPCR assays were developed for use in this study. Both assays target the *T. arcticus* cytochrome oxidase subunit 1 gene (cox1) and share the same reverse primer. The first unique set of forward primer and positive-sense strand probe produces a 128 bp amplicon while the second set produces a 468 bp amplicon. In silico validation was performed by aligning all available *T. arcticus* cox1 gene from NCBI and BOLD databases and identifying conserved regions of DNA greater than 15 base pairs in length. We then used NCBI's nucleotide BLAST to remove areas with high similarity to any off-target sequences. The primer sequences that were selected with the appropriate thermal properties minimized similarity with sequences outside of the *Thymallus* genus. The only teleost fish (outside of the *Thymallus* genus) with fewer than three base pair mismatches with at least one primer was *Liopropoma olneyi*, a Caribbean reef fish. NCBI Primer-BLAST was used to confirm this result in the nucleotide (nr) database of teleost fishes using default stringency and specificity settings. Notably, while the assays designed here can reliably detect *T. arcticus*, there is also significant sequence similarity with other members of the *Thymallus* genus. Therefore, these assays should not be considered species specific when used in water bodies that may contain other members of *Thymallus*.

Each assay's annealing temperature was optimized using temperature-gradient qPCR (from 58 to 67 °C), wherein the optimal annealing temperature was that which minimized the *Cq* when amplifying replicate synthetic DNA standards of 5000 gene copies. The optimal primer ratios were determined similar to Wilcox et al. (2015). The limit of detection (LOD) and limit of quantification (LOQ) were determined in both an ideal sample matrix (i.e., molecular grade water) and in a relevant sample matrix (extracted water from the study creek) using the eLowQuant method of Lesperance et al. (2021).

The assays were validated in vitro with DNA extracted from *T. arcticus* from the study creek and from tissues of regional origin of *Salvelinus fontinalis*, which do occur in our study reach, and other salmonids found in nearby waters including *Oncorhynchus mykiss, O. clarkii bouvieri, O. clarkii lewisi, Salmo trutta,* and

Prosopium williamsoni. Tissue validation was performed with 10 replicates each. *In situ* validation was performed on eDNA water samples collected from the brood stock reservoir (known positive source) and from the study creek water collected above the barrier prior to the start of the experiment (known negative source).

Results: assay comparison

We observed substantially higher detection and copy number measurements using the short amplicon compared to the long amplicon assay. For the long amplicon assay, 37.5% of replicates were nondetections and 32.1% of samples failed to detect eDNA across all 5 replicates, compared to 6.2 and 3.8%, respectively, for the short amplicon assay. The short amplicon replicate-level quantitative data ranged from 1.71 to 4.90 $\log_{10}$ copies/L and −0.29 to 2.90 $\log_{10}$ copies/reaction and the long amplicon replicate-level quantitative data ranged from 2.22 to 5.91 $\log_{10}$ copies/L and 0.22 to 3.91 $\log_{10}$ copies/reaction. Due to the poorer performance of the long amplicon assay, we used the short amplicon assay data for analysis.

Methods: DNA extraction

All eDNA and tissue samples were extracted with Qiagen DNeasy Blood and Tissue Kits (cat. #69504) with Qiagen DNeasy Lyse and Spin Baskets (cat. #19598) with minimal alterations of the manufacturer's protocol. DNA was eluted in 400 µL of Qiagen Buffer AE. All DNA extraction batches included an extraction negative control using only extraction kit reagents. These extraction blanks were otherwise handled and analyzed identically to samples.

Methods: quantitative PCR

Assays were run on a BioRad CFX 96-Touch or BioRad Opus thermal cycler (Hercules, CA). Reactions took place in BioRad Hard-Shell®optical 96-well plates (cat. #HSP9601) sealed with BioRad Microseal®optical adhesive film (cat. #MSC1001). The thermal cycle was: 95 °C for 15 min then 50 cycles of 94 °C for 15 s and 60 °C for 60 s. Reactions of 20 µL included 10 µL of Qiagen Quantitect Master Mix, 3 µL sterile water, 0.5 µM of forward and 0.4 µM of reverse primer, 0.25 µM FAM-labeled hydrolysis probe, and 4 µL of DNA extract. The two *T. arcticus* assays were not multiplexed together, but were run in separate reactions multiplexed with an internal positive control (IPC, see below). Every 96-well plate run as part of this study had the same duplicated (two replicates) controls: six point 1:10 dilution *T. arcticus* synthetic standard curve ranging from 4e0 to 4e5 target DNA copies, no-template control (NTC), and internally blocked negative control (IBC). FAM and VIC fluorescence values were ROX-normalized prior to baseline correction and amplification detection (Patrone et al. 2020) using R v4.0.3 statistical software (R Core Team 2021). Successful amplification of DNA was defined as any curve for which a feasible solution with less than 10% transformation error was found for the non-linear optimization transformation presented in Patrone et al. (2020).

Supplementary Information The online version contains supplementary material available at https://doi.org/10.1007/s10651-024-00632-8.

Acknowledgements We thank Diogo Bolster for recommending the power law removal model over the Weibull to provide a similar fit with one less parameter and Andy Royle, Qing Zhao, Christian Stratton, and two anonymous reviewers for reviewing a previous version of this manuscript. Any use of trade, firm, or product names is for descriptive purposes only and does not imply endorsement by the U.S. Government.

Disclaimer This draft manuscript is distributed solely for the purposes of scientific peer review, so this must not be disclosed or released by reviewers. Because the manuscript has not yet been approved for publication by the U.G. Geological Survey (USGS), it does not represent any official USGS finding or policy.

Author contributions AS and PH conceived and designed the experiment. BA led model development, data analysis, and the writing of the manuscript. PH and AS contributed to model development and data analysis. PH performed all laboratory analyses. All authors contributed to data collection and writing the manuscript.

Declarations

Conflict of interest We have no conflicts of interest to report.

Open research statement Data and code are provided at: https://datadryad.org/stash/share/YSe7cJkr8wL8g4qhs7wFeKm5LLRD8qcw1sHFOg57v4c.

References

Altermatt F, Carraro L, Antonetti M, Albouy C, Zhang Y, Lyet A, Zhang X, Pellissier L (2023) Quantifying biodiversity using eDNA from water bodies: general principles and recommendations for sampling designs. Environ DNA 5(4):671–682

Ariyo O, Quintero A, Muñoz J, Verbeke G, Lesaffre E (2020) Bayesian model selection in linear mixed models for longitudinal data. J Appl Stat 47(5):890–913

Ariyo O, Lesaffre E, Verbeke G, Quintero A (2022) Model selection for Bayesian linear mixed models with longitudinal data: sensitivity to the choice of priors. Commun Stat Simul Comput 51(4):1591–1615

Brooks SP, Gelman A (1998) General methods for monitoring convergence of iterative simulations. J Comput Graph Stat 7(4):434–455

Burian A, Mauvisseau Q, Bulling M, Domisch S, Qian S, Sweet M (2021) Improving the reliability of eDNA data interpretation. Mol Ecol Resour 21(5):1422–1433

Bustin S, Hugget J (2017) qPCR primer design revisited. Biomol Detect Quantification 14:19–28

Bylemans J, Furlan EM, Gleeson DM, Hardy CM, Duncan RP (2018) Does size matter? An experimental evaluation of the relative abundance and decay rates of aquatic environmental DNA. Environ Sci Technol 52(11):6408–6416

Carraro L, Hartikainen H, Jokela J, Bertuzzo E, Rinaldo A (2018) Estimating species distribution and abundance in river networks using environmental DNA. Proc Natl Acad Sci USA 115(46):11724–11729

Carraro L, Stauffer JB, Altermatt F (2021) How to design optimal eDNA sampling strategies for biomonitoring in river networks. Environ DNA 3(1):157–172

Carraro L, Blackman RC, Altermatt F (2023) Modelling environmental DNA transport in rivers reveals highly resolved spatio-temporal biodiversity patterns. Sci Rep 13(1):8854

Chambert T, Pilliod DS, Goldberg CS, Doi H, Takahara T (2018) An analytical framework for estimating aquatic species density from environmental DNA. Ecol Evol 8(6):3468–3477

Chik AHS, Schmidt PJ, Emelko MB (2018) Learning something from nothing: the critical importance of rethinking microbial non-detects. Front Microbiol 9:2304

Conn PB, Johnson DS, Williams PJ, Melin SR, Hooten MB (2018) A guide to Bayesian model checking for ecologists. Ecol Monogr 88(4):526–542

Curtis AN, Tiemann JS, Douglass SA, Davis MA, Larson ER (2021) High stream flows dilute environmental DNA (eDNA) concentrations and reduce detectability. Divers Distrib 27(10):1918–1931

David GK, Mitchel K (2012) Survival analysis: a Self-Learning text. Springer, Berlin

de Valpine P, Turek D, Paciorek CJ, Anderson-Bergman C, Lang DT, Bodik R (2017) Programming with models: writing statistical algorithms for general model structures with NIMBLE. J Comput Graph Stat 26(2):403–413

Dorazio RM, Erickson RA (2018) eDNAoccupancy: an R package for multiscale occupancy modelling of environmental DNA data. Mol Ecol Resour 18(2):368–380

Dorazio RM, Hunter ME (2015) Statistical models for the analysis and design of digital polymerase chain reaction (DPCR) experiments. Anal Chem 87(21):10886–10893

Dube S, Qin J, Ramakrishnan R (2008) Mathematical analysis of copy number variation in a DNA sample using digital PCR on a nanofluidic device. PLoS ONE 3(8):e2876

Ellison SL, English CA, Burns MJ, Keer JT (2006) Routes to improving the reliability of low level DNA analysis using real-time PCR. BMC Biotechnol 6(1):1–11

Espe MB, Johnston M, Blankenship SM, Dean CA, Bowen MD, Schultz A, Schumer G (2022) The Artemis package for environmental DNA analysis in R. Environ DNA 4(3):523–532

Ferguson PF, Conroy MJ, Hepinstall-Cymerman J (2015) Occupancy models for data with false positive and false negative errors and heterogeneity across sites and surveys. Methods Ecol Evol 6(12):1395–1406

Furlan EM, Gleeson D, Hardy CM, Duncan RP (2016) A framework for estimating the sensitivity of eDNA surveys. Mol Ecol Resour 16(3):641–654

Gelman A, Rubin DB (1992) Inference from iterative simulation using multiple sequences. Stat Sci 7(4):457–472

Gelman A, Meng X-L, Stern H (1996) Posterior predictive assessment of model fitness via realized discrepancies. Stat Sin 6(4):733–760

Gelman A, Carlin JB, Stern HS, Rubin DB (2013) Bayesian data analysis, 3rd edn. Chapman and Hall/CRC, New York

Gelman A, Hwang J, Vehtari A (2014) Understanding predictive information criteria for Bayesian models. Stat Comput 24(6):997–1016

Goldberg CS, Turner CR, Deiner K, Klymus KE, Thomsen PF, Murphy MA, Spear SF, McKee A, Oyler-McCance SJ, Cornman RS, Laramie MB, Mahon AR, Lance RF, Pilliod DS, Strickler KM, Waits LP, Fremier AK, Takahara T, Herder JE, Taberlet P (2016) Critical considerations for the application of environmental DNA methods to detect aquatic species. Methods Ecol Evol 7:1299–1307

Guillera-Arroita G, Lahoz-Monfort JJ, van Rooyen AR, Weeks AR, Tingley R (2017) Dealing with false-positive and false-negative errors about species occurrence at multiple levels. Methods Ecol Evol 8(9):1081–1091

Harrison JB, Sunday JM, Rogers SM (2019) Predicting the fate of eDNA in the environment and implications for studying biodiversity. Proc R Soc B 286(1915):20191409

Hartman LJ, Coyne SR, Norwood DA (2005) Development of a novel internal positive control for Taqman® based assays. Mol Cell Probes 19(1):51–59

Herschy R (1993) The velocity–area method. Flow Meas Instrum 4(1):7–10

Hunter ME, Oyler-McCance SJ, Dorazio RM, Fike JA, Smith BJ, Hunter CT, Reed RN, Hart KM (2015) Environmental DNA (eDNA) sampling improves occurrence and detection estimates of invasive Burmese pythons. PLoS ONE 10(4):e0121655

Hunter ME, Dorazio RM, Butterfield JS, Meigs-Friend G, Nico LG, Ferrante JA (2017) Detection limits of quantitative and digital PCR assays and their influence in presence–absence surveys of environmental DNA. Mol Ecol Resour 17(2):221–229

Hunter ME, Ferrante JA, Meigs-Friend G, Ulmer A (2019) Improving eDNA yield and inhibitor reduction through increased water volumes and multi-filter isolation techniques. Sci Rep 9(1):5259

Jane SF, Wilcox TM, McKelvey KS, Young MK, Schwartz MK, Lowe WH, Letcher BH, Whiteley AR (2015) Distance, flow and PCR inhibition: eDNA dynamics in two headwater streams. Mol Ecol Resour 15(1):216–227

Journal : SmallExtended 10651	Article No : 632	Pages : 36	MS Code : 632	Dispatch : 13-11-2024

Jo T, Yamanaka H (2022) Meta-analyses of environmental DNA downstream transport and deposition in relation to hydrogeography in riverine environments. Freshw Biol 67(8):1333–1343

Kelly RP, Lodge DM, Lee KN, Theroux S, Sepulveda AJ, Scholin CA, Craine JM, Andruszkiewicz Allan E, Nichols KM, Parsons KM et al (2023) Toward a national eDNA strategy for the United States. Environ DNA 6(1):e432

King R, Morgan B, Gimenez O, Brooks S (2009) Bayesian analysis for population ecology. CRC Press, Boca Raton

Klymus KE, Merkes CM, Allison MJ, Goldberg CS, Helbing CC, Hunter ME, Jackson CA, Lance RF, Mangan AM, Monroe EM et al (2020) Reporting the limits of detection and quantification for environmental DNA assays. Environ DNA 2(3):271–282

Kontanis EJ, Reed FA (2006) Evaluation of real-time PCR amplification efficiencies to detect PCR inhibitors. J Forensic Sci 51(4):795–804

Kvålseth TO (2017) Coefficient of variation: the second-order alternative. J Appl Stat 44(3):402–415

Lance RF, Guan X (2020) Variation in inhibitor effects on QPCR assays and implications for eDNA surveys. Can J Fish Aquat Sci 77(1):23–33

Lance RF, Klymus KE, Richter CA, Guan X, Farrington HL, Carr MR, Thompson N, Chapman DC, Baerwaldt KL (2017) Experimental observations on the decay of environmental DNA from bighead and silver carps. Manag Biol Invasions 8(3):343–359

Laporte M, Bougas B, Côté G, Champoux O, Paradis Y, Morin J, Bernatchez L (2020) Caged fish experiment and hydrodynamic bidimensional modeling highlight the importance to consider 2D dispersion in fluvial environmental DNA studies. Environ DNA 2(3):362–372

Larson ER, Graham BM, Achury R, Coon JJ, Daniels MK, Gambrell DK, Jonasen KL, King GD, LaRacuente N, Perrin-Stowe TI et al (2020) From eDNA to citizen science: emerging tools for the early detection of invasive species. Front Ecol Environ 18(4):194–202

Lesperance ML, Allison MJ, Bergman LC, Hocking MD, Helbing CC (2021) A statistical model for calibration and computation of detection and quantification limits for low copy number environmental DNA samples. Environ DNA 3(5):970–981

Levi T, Allen JM, Bell D, Joyce J, Russell JR, Tallmon DA, Vulstek SC, Yang C, Yu DW (2019) Environmental DNA for the enumeration and management of Pacific salmon. Mol Ecol Resour 19(3):597–608

McClintock BT, Bailey LL, Pollock KH, Simons TR (2010) Unmodeled observation error induces bias when inferring patterns and dynamics of species occurrence via aural detections. Ecology 91(8):2446–2454

McKee AM, Spear SF, Pierson TW (2015) The effect of dilution and the use of a post-extraction nucleic acid purification column on the accuracy, precision, and inhibition of environmental DNA samples. Biol Conserv 183:70–76

Meredith M, Kruschke J (2020) HDInterval: highest (posterior) density intervals. R package version 0.2, 2

Merkle EC, Furr D, Rabe-Hesketh S (2019) Bayesian comparison of latent variable models: conditional versus marginal likelihoods. Psychometrika 84:802–829

Morisette J, Burgiel S, Brantley K, Daniel WM, Darling J, Davis J, Franklin T, Gaddis K, Hunter M, Lance R et al (2021) Strategic considerations for invasive species managers in the utilization of environmental DNA (eDNA): steps for incorporating this powerful surveillance tool. Manag Biol Invasions Int J Appl Res Biol Invasions 12(3):747

Nichols JD, Bailey LL, O'Connell AF Jr, Talancy NW, Campbell Grant EH, Gilbert AT, Annand EM, Husband TP, Hines JE (2008) Multi-scale occupancy estimation and modelling using multiple detection methods. J Appl Ecol 45(5):1321–1329

Opel KL, Chung D, McCord BR (2010) A study of PCR inhibition mechanisms using real time PCR. J Forensic Sci 55(1):25–33

Papaspiliopoulos O, Roberts GO, Sköld M (2007) A general framework for the parametrization of hierarchical models. Stat Sci 22(1):59–73

Patrone PN, Kearsley AJ, Majikes JM, Liddle JA (2020) Analysis and uncertainty quantification of DNA fluorescence melt data: applications of affine transformations. Anal Biochem 607:113773

Ponisio LC, de Valpine P, Michaud N, Turek D (2020) One size does not fit all: customizing MCMC methods for hierarchical models using NIMBLE. Ecol Evol 10(5):2385–2416

R Core Team (2021) R: a language and environment for statistical computing. R Foundation for Statistical Computing, Vienna. https://www.R-project.org/

Rees HC, Maddison BC, Middleditch DJ, Patmore JR, Gough KC (2014) Review: the detection of aquatic animal species using environmental DNA—a review of eDNA as a survey tool in ecology. J Appl Ecol 51:1450–1459

Rossmanith P, Wagner M (2011) A novel Poisson distribution-based approach for testing boundaries of real-time PCR assays for food pathogen quantification. J Food Prot 74(9):1404–1412

Rourke ML, Fowler AM, Hughes JM, Broadhurst MK, DiBattista JD, Fielder S, Wilkes Walburn J, Furlan EM (2022) Environmental DNA (eDNA) as a tool for assessing fish biomass: a review of approaches and future considerations for resource surveys. Environ DNA 4(1):9–33

Royle JA, Dorazio RM (2008) Hierarchical modeling and inference in ecology: the analysis of data from populations, metapopulations and communities. Elsevier, Amsterdam

Royle JA, Nichols JD (2003) Estimating abundance from repeated presence–absence data or point counts. Ecology 84(3):777–790

Sansom BJ, Sassoubre LM (2017) Environmental DNA (eDNA) shedding and decay rates to model freshwater mussel eDNA transport in a river. Environ Sci Technol 51(24):14244–14253

Searcy RT, Boehm AB, Weinstock C, Preston CM, Jensen S, Roman B, Birch JM, Scholin CA, Van Houtan KS, Kiernan JD et al (2022) High-frequency and long-term observations of eDNA from imperiled salmonids in a coastal stream: temporal dynamics, relationships with environmental factors, and comparisons with conventional observations. Environ DNA 4(4):776–789

Sepulveda AJ, Nelson NM, Jerde CL, Luikart G (2020a) Are environmental DNA methods ready for aquatic invasive species management? Trends Ecol Evol 35(8):668–678

Sepulveda AJ, Hutchins PR, Jackson C, Ostberg C, Laramie MB, Amberg J, Counihan T, Hoegh A, Pilliod DS (2020b) A round-robin evaluation of the repeatability and reproducibility of environmental DNA assays for Dreissenid mussels. Environ DNA 2(4):446–459

Sepulveda AJ, Dumoulin CE, Blanchette DL, McPhedran J, Holme C, Whalen N, Hunter ME, Merkes CM, Richter CA, Neilson ME et al (2023) When are environmental DNA early detections of invasive species actionable? J Environ Manag 343:118216

Shelton AO, Kelly RP, O'Donnell JL, Park L, Schwenke P, Greene C, Henderson RA, Beamer EM (2019) Environmental DNA provides quantitative estimates of a threatened salmon species. Biol Conserv 237:383–391

Shogren AJ, Tank JL, Andruszkiewicz E, Olds B, Mahon AR, Jerde CL, Bolster D (2017) Controls on eDNA movement in streams: transport, retention, and resuspension. Sci Rep 7(1):5065

Sidstedt M, Rådström P, Hedman J (2020) PCR inhibition in QPCR, DPCR and MPS-mechanisms and solutions. Anal Bioanal Chem 412(9):2009–2023

Smith MM, Goldberg CS (2020) Occupancy in dynamic systems: accounting for multiple scales and false positives using environmental DNA to inform monitoring. Ecography 43(3):376–386

Snyder ED, Tank JL, Brandão-Dias PF, Bibby K, Shogren AJ, Bivins AW, Peters B, Curtis EM, Bolster D, Egan SP et al (2023) Environmental DNA (eDNA) removal rates in streams differ by particle size under varying substrate and light conditions. Sci Total Environ 903:166469

Stratton C, Sepulveda AJ, Hoegh A (2020) MSOCC: fit and analyse computationally efficient multi-scale occupancy models in R. Methods Ecol Evol 11(9):1113–1120

Tellinghuisen J (2020) DPCR vs. QPCR: the role of Poisson statistics at low concentrations. Anal Biochem 611:113946

Tillotson MD, Kelly RP, Duda JJ, Hoy M, Kralj J, Quinn TP (2018) Concentrations of environmental DNA (eDNA) reflect spawning salmon abundance at fine spatial and temporal scales. Biol Conserv 220:1–11

Tran M-N, Scharth M, Gunawan D, Kohn R, Brown SD, Hawkins GE (2021) Robustly estimating the marginal likelihood for cognitive models via importance sampling. Behav Res Methods 53:1148–1165

Troth CR, Sweet MJ, Nightingale J, Burian A (2021) Seasonality, DNA degradation and spatial heterogeneity as drivers of eDNA detection dynamics. Sci Total Environ 768:144466

Volkmann H, Schwartz T, Kirchen S, Stofer C, Obst U (2007) Evaluation of inhibition and cross-reaction effects on real-time PCR applied to the total DNA of wastewater samples for the quantification of bacterial antibiotic resistance genes and taxon-specific targets. Mol Cell Probes 21(2):125–133

Watanabe S, Opper M (2010) Asymptotic equivalence of Bayes cross validation and widely applicable information criterion in singular learning theory. J Mach Learn Res 11(12):3571–3594

Wilcox TM, Carim KJ, McKelvey KS, Young MK, Schwartz MK (2015) The dual challenges of generality and specificity when developing environmental DNA markers for species and subspecies of *Oncorhynchus*. PLoS ONE 10(11):e0142008

Journal : SmallExtended 10651	Article No : 632	Pages : 36	MS Code : 632	Dispatch : 13-11-2024

Wood ZT, Erdman BF, York G, Trial JG, Kinnison MT (2020) Experimental assessment of optimal lotic eDNA sampling and assay multiplexing for a critically endangered fish. Environ DNA 2(4):407–417

Wood ZT, Lacoursière-Roussel A, LeBlanc F, Trudel M, Kinnison MT, Garry McBrine C, Pavey SA, Gagné N (2021) Spatial heterogeneity of eDNA transport improves stream assessment of threatened salmon presence, abundance, and location. Front Ecol Evol 9:650717

Yao M, Zhang S, Lu Q, Chen X, Zhang S-Y, Kong Y, Zhao J (2022) Fishing for fish environmental DNA: ecological applications, methodological considerations, surveying designs, and ways forward. Mol Ecol 31(20):5132–5164

Yates MC, Fraser DJ, Derry AM (2019) Meta-analysis supports further refinement of eDNA for monitoring aquatic species-specific abundance in nature. Environ DNA 1(1):5–13

Yates MC, Cristescu ME, Derry AM (2021a) Integrating physiology and environmental dynamics to operationalize environmental DNA (eDNA) as a means to monitor freshwater macro-organism abundance. Mol Ecol 30(24):6531–6550

Yates MC, Glaser D, Post JR, Cristescu ME, Fraser DJ, Derry AM (2021b) The relationship between eDNA particle concentration and organism abundance in nature is strengthened by allometric scaling. Mol Ecol 30(13):3068–3082

Yates M, Gaudet-Boulay M, Garcia Machado E, Côté G, Gilbert A, Bernatchez L (2023) How much is enough? Examining the sampling effort necessary to estimate mean eDNA concentrations in lentic systems. Environ DNA 5(6):1527–1540

Authors and Affiliations

Ben C. Augustine[1] · Patrick R. Hutchins[1] · Devin N. Jones[1] · Jacob R. Williams[2] · Eric Leinonen[2] · Adam J. Sepulveda[1]

✉ Ben C. Augustine
baugustine@usgs.gov

[1] Northern Rocky Mountain Science Center, U.S. Geological Survey, 2327 University Way Suite 2, Bozeman, MT 59715, USA

[2] Natural Resources Program, Turner Institute of Ecoagriculture, 901 Technology Blvd, Bozeman, MT 59718, USA